FISEVIER

Contents lists available at ScienceDirect

Quaternary Science Reviews

journal homepage: www.elsevier.com/locate/quascirev



The large MIS 4 and long MIS 2 glacier maxima on the southern tip of South America



Carly Peltier ^{a, b, *}, Michael R. Kaplan ^b, Sean D. Birkel ^c, Rodrigo L. Soteres ^{d, e}, Esteban A. Sagredo ^{d, e, f}, Juan Carlos Aravena ^g, José Araos ^h, Patricio I. Moreno ^{i, e}, Roseanne Schwartz ^b, Joerg M. Schaefer ^{a, b}

- ^a Department of Earth and Environmental Sciences, Columbia University, New York, NY, 10027, USA
- ^b Geochemistry, Lamont-Doherty Earth Observatory, Columbia University, Palisades, NY, 10964, USA
- ^c Climate Change Institute & School of Earth and Climate Sciences, University of Maine, Orono, ME, 04469, USA
- d Instituto de Geografía, Pontificia Universidad Católica de Chile, Santiago, Chile
- e Millennium Nucleus Paleoclimate, Universidad de Chile, Santiago, Chile
- f Estación Patagonia de Investigaciones Interdisciplinarias UC, Pontificia Universidad Católica de Chile, Santiago, Chile
- g Centro de Investigación Gaia Antártica, Universidad de Magallanes, Punta Arenas, Chile
- ^h Departamento de Geografía, Facultad de Cs. Sociales, Universidad Alberto Hurtado, Cienfuegos 41, Santiago, Chile
- ⁱ Institute of Ecology and Biodiversity, Department of Ecological Sciences, Universidad de Chile, Santiago, Chile

ARTICLE INFO

Article history:
Received 10 September 2020
Received in revised form
8 February 2021
Accepted 16 February 2021
Available online 11 May 2021

Handling Editor: C. O'Cofaigh

Keywords:
Pleistocene
Glaciation
Paleoclimatology
South America
Patagonia
Paleo ice sheet modeling
MIS 4
MIS 2
Glacial geomorphology
10Be exposure Dating

ABSTRACT

Robust glacial chronologies are needed to address the fundamental questions of when and why Ice Age climates begin and end. Well-preserved glacial deposits left by large ice sheet lobes adjacent to Estrecho de Magallanes (53°S; Chile) in southernmost South America provide a unique opportunity to reconstruct the timing and fine structure of the last two major glaciations, as well as the last termination. We present a new precise ¹⁰Be surface exposure dataset of 34 moraine boulders directly tied to a recently published, high resolution glacial geomorphic map of the deposits left by the Magallanes lobe.

We find that the southern section of the Patagonian Ice Sheet was more extensive during Marine Isotope Stage 4 (MIS 4) than during MIS 2, representing the first direct dating of the MIS 4 glacier culmination in South America, Similar to the MIS 2 glacial maxima, within MIS 4 there were multiple advances that we date (n = 6 samples) to between 67.5 ± 2.1 and 62.1 ± 2.0 ka. A similarly timed MIS 4 advance was identified in New Zealand, indicating that this is a hemisphere-wide glacier-climate signal, which is further corroborated by South Atlantic and Pacific temperature proxy records. Inboard of the MIS 4 moraine complex, we date a sequence of geomorphically distinct MIS 2 moraines that represent separate major periods of glacial stability. The MIS 2 maximum extent occurred by 27.4 ± 0.8 ka (n = 4; arithmetic mean, with the standard error of the mean and 3% propagated production rate error) and was followed by at least four more full glacial culminations at 25.7 ± 0.8 (n = 3), 23.9 ± 0.8 (n = 5), 19.1 ± 0.7 (n = 3), and 18.1 ± 0.6 ka (n = 3), which represent periods when the glacier was in equilibrium with the climate for long enough to form major moraines. About 18 km inboard, this sequence is followed by smaller-scale recessional moraine crests, deposited on drumlinized terrain rather than a moraine drift, that we date to 18.0 ± 0.8 ka, indicating the glacier was in net retreat at this time. Tentative results from a 2D ice sheet model suggest that the Magallanes lobe may have reached mapped inner and outer MIS 2 moraines from a climate with approximately 4.5 °C and 5.5 °C cooler summers, respectively, assuming ~25% less annual precipitation, relative to modern climate. We hypothesize that during the last glacial cycle, shifts in the subtropical and subantarctic fronts, and related ocean-atmosphere patterns, explain MIS 4 to 2 glacial behavior in the southern mid-latitudes.

© 2021 Elsevier Ltd. All rights reserved.

E-mail address: cpeltier@ldeo.columbia.edu (C. Peltier).

^{*} Corresponding author. Geochemistry, LDEO, Columbia University, Palisades, NY, 10964, USA.

1. Introduction

The last glacial maximum (LGM; ~26,000-19,000 years ago, Clark et al., 2009) has been a major focus of study in paleoclimatology because it allows us to peer into a not-so-distant past, one reachable by radiocarbon dating, where Earth's climate was very different from today. Knowledge of LGM climates, how fast they changed, and what caused those changes remain as fundamental questions, the answers to which will (1) allow improved understanding of how the climate system operates, and (2) help constrain numerical models used to make predictions for the future. Marine benthic $\delta^{18}O$ and sea level records have been instrumental in deciphering past climate changes (e.g., CLIMAP, 1976; 1981; Mix et al., 2001; Lisiecki and Raymo, 2005); however, these records are globally or regionally integrated by nature, meaning they are of limited use for mapping the worldwide fingerprint of the LGM, and directly documenting the changes on land (Clark et al., 2009). Moreover, glacial records from the last glacial cycle show that glaciers and ice sheets reached their maximum extents at different points and at multiple times within marine isotope stages (MIS) 2, 3, and 4 (e.g., Hughes et al., 2013), calling into question the nature and structure of the LGM.

Furthermore, according to Milankovitch theory, glacial cycles result from changes in Northern Hemisphere summer solar insolation intensity paired with internal feedbacks (Milankovitch, 1941). There is ample evidence showing the rate of change of globally integrated ice volume is well correlated with Northern Hemisphere insolation intensity with little to no lag (Hays et al., 1976; Roe, 2006). However, summer insolation intensity is out of phase between the two hemispheres, meaning that if insolation were the singular control on glacier flux, while Northern Hemisphere glaciers expand, Southern Hemisphere glaciers would retreat, a problem that Mercer described as "a fly in the ointment of the Milankovitch theory" (Broecker, 1978; Mercer, 1984).

Two main problems have made it difficult to reconstruct spatial differences in glacier and ice sheet maxima through the last glacial cycle, and in particular the structure of MIS 2, in order to evaluate fully the "fly in the ointment". First, denudation or LGM glacial advances have destroyed the terrestrial records formed from previous glaciations in many places, so only the deposits from a fraction of a glacial cycle are preserved on land (termed "obliterative overlap" by Gibbons et al., 1984). Pre-LGM dated terrestrial glacial deposits are particularly rare in the Southern Hemisphere, in part because Antarctic glaciers reached the continental shelf edge, resulting in stratigraphically complex deposits on the continental slope. Second, where terrestrial glacial records are preserved, difficulties in dating these deposits have prevented precise correlation to potential forcing mechanisms. Until the development of the ¹⁰Be method, radiocarbon was the main tool for dating glacial events. However, the ~40 ka (thousands of years before the present, a point in time relative to AD 1950) radiocarbon limit means that we can only date deposits back to MIS 3 (57-29 ka; all references to the timing of marine isotope stages are from Lisiecki and Raymo, 2005), making it impossible to tackle questions that require the study of multiple glaciations. Moreover, within the radiocarbon limit, there is often a lack of organic material in glacial tills and in periglacial environments, meaning that we can only provide minimum and maximum ages for a glacial advance by dating organic material stratigraphically above and below the glacial deposit, where the latter is rarely preserved.

The deposits left by large lobes of the Patagonian Ice Sheet (PIS) provide us with a unique opportunity to evaluate the precise timing of Southern Hemisphere glaciation, in order to contribute to answering the fundamental questions of when and why glacial cycles occur. The PIS was the largest Southern Hemisphere glacier

outside of Antarctica and in general experienced progressively smaller glacier extents throughout the last million years. Unlike in Europe or North America where the Mid-Pleistocene terrestrial glacial record is more complex, land terminating glacier lobes of the PIS left behind well-developed, nested moraine sequences. At Estrecho de Magallanes we find a long sequence of uniquely wellpreserved moraines that allow us to map and date many glacial stillstands, beyond the LGM, so that we can address the first problem laid out above. Improvements in the ¹⁰Be dating method (Schaefer et al., 2009) and the development of a local production rate (Kaplan et al., 2011) allow us to date directly the advances with unprecedented accuracy and precision, with errors of ~2-4%, addressing the second problem laid out above. The production of a new high-resolution geomorphic map (Soteres et al., 2020) allows us to group the ages by landform, and to interpret our ages as direct dates of glacier advance. Here we present a precise record of the sub-millennial scale timing of glacial maxima during MIS 2 (29-14 ka), as well as the first direct dating of a MIS 4 (71-57 ka) glacier advance in southern South America. The new findings indicate that the PIS was as large if not larger during MIS 4 than MIS 2, and multiple advances occurred during both major glacier expansions.

2. Modern setting and climate

The Estrecho de Magallanes in Chile connects the Pacific and Atlantic oceans, separating Isla Grande de Tierra del Fuego from the rest of the continent. At 53°S, 70°W, the site sits just north of the modern mean position of the Subantarctic Front, which hugs the southern tip of South America (Fig. 1).

Modern climate at Estrecho de Magallanes is maritime. Mean annual temperature in Punta Arenas on the western side of Estrecho de Magallanes is ~6.5 °C (Garreaud et al., 2013). The area has a sharp year-round W-E precipitation gradient due to orographic precipitation on the west side of the Andes Cordillera and a rain shadow on the east. Punta Arenas receives a mean annual precipitation of ~440–500 mm/yr (Zamora and Santana, 1979; Schneider et al., 2003), while precipitation <150 km to the west, near Gran Campo Nevado at sea level is ~13x greater (6600 mm/yr; Schneider et al., 2003). Precipitation in the cordillera is positively correlated with westerly wind speed, while the opposite is true to the east at Estrecho de Magallanes (Moreno et al., 2018a).

The glacier lobe that once filled Estrecho de Magallanes accumulated in Cordillera Darwin and formed part of the PIS. The bedrock surface of Cordillera Darwin contains mainly the Cordillera Darwin metamorphic complex, Beagle and Darwin granite suites, and the Tobífera Formation (rhyolitic volcanic rocks; Hervé et al., 2010). Consequently, the erratics around Estrecho de Magallanes have a wide range of lithologies, which makes some areas in this sector hard to date with the ¹⁰Be method.

3. Background

3.1. Prior research in the Estrecho de Magallanes area

The glacial geomorphology of the area has been mapped by several research teams with varying degrees of detail and precision (Benn and Clapperton, 2000; Bentley et al., 2005; Lovell et al., 2011; Darvill et al., 2014). Recently, Soteres et al. (2020) mapped, in unprecedented detail, a sequence of six major right lateral and frontal moraines in the eastern sector of Estrecho de Magallanes that we focus on in this study. The overall shape of the moraines is slightly sinuous (Fig. 2A), where the moraines in the area in which we focus the chronology (Fig. 2C) form a stretched-out "C" shape.

Building on the work of Caldenius (1932), Porter (1990), Porter et al. (1992), and Meglioli (1992) among others, Clapperton et al.

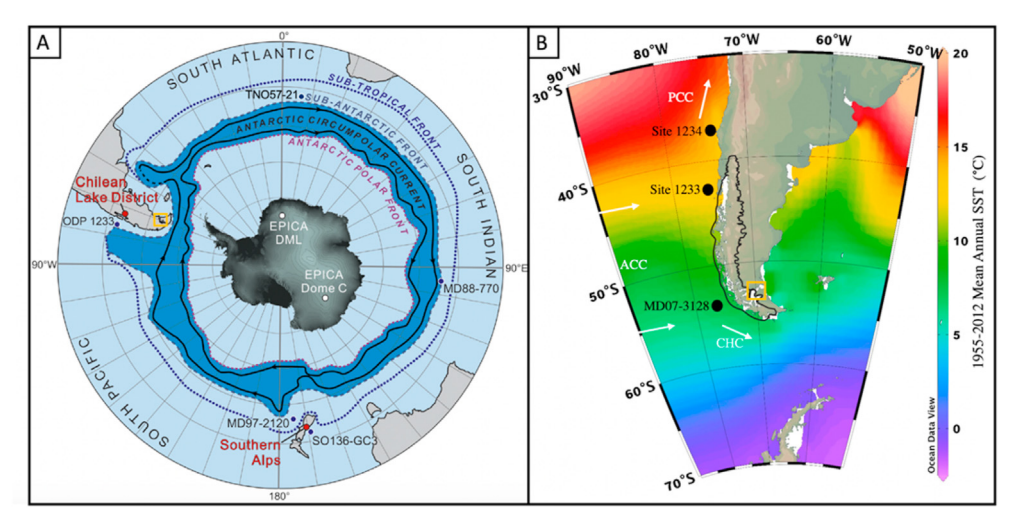


Fig. 1. Location of study site (yellow square) in the context of modern Southern Hemisphere oceanography. A) From Kelley et al. (2014). B) 1955–2012 mean annual sea surface temperature (Locarnini et al., 2010) with schematic representations of the locations of the Perú Chile Current (PCC), Antarctic Circumpolar Current (ACC), Cape Horn Current (CHC) based off Caniupán et al. (2011); black outline represents inferred extent of the Patagonian Ice Sheet during the local LGM. (For interpretation of the references to color in this figure legend, the reader is referred to the Web version of this article.)

(1995) proposed that five advances occurred during the last glacial cycle, named A-E where A is pre-LGM and E is late-glacial (Fig. 2A). Based on maximum-limiting amino-acid epimerization dating (and infinite radiocarbon ages) of shells from a deposit thought to be basal till of the outermost limit (advance A), they concluded it may have been deposited during ~MIS 5 or 4 (Clapperton et al., 1995). Glacial retreat took place between this outermost advance and the subsequent MIS 2 advance, as evidenced by shelly basal till indicating there was a marine incursion into the strait (Clapperton et al., 1995). They proposed the MIS 2 maximum terminated on Península Juan Mazía (advances B and C), followed by advance D, which terminated on Punta Paulo (Fig. 2A). They did not find shell fragments in the till associated with the D limit, indicating that a marine ingression may not have taken place between the event C and advance D.

Following this work and maintaining the A-E classification scheme of Clapperton et al., McCulloch et al. (2005b) were the first to apply cosmogenic exposure dating to the Magallanes lobe as well as the adjacent Bahía Inútil lobe, which they paired with tephrochronology, amino acid data, and carefully prepared samples for radiocarbon dating given the presence of reworked pre-Quaternary lignite in the area. They found that the Magallanes lobe was most extensive after ~31 cal ka BP (thousands of calendar years before present), as radiocarbon dating of shells from a diamict associated with advance B produced ages ranging from ~44.8 to 31.3 cal ka BP (McCulloch et al., 2005b). The authors reported three ¹⁰Be dates for this advance with ages of 29.3 \pm 1.7, 27.4 \pm 2.3, and 26.1 \pm 0.9 ka (all of the cosmogenic ages from previous work presented in our study have been recalculated with updated systematics, as explained below, and the mean ages are shown with the standard error of the mean (SEM) and local production rate uncertainty propagated). This is followed by an advance before ~21.8-20.4 cal ka BP (based on a radiocarbon date from outside of Porvenir; advance C), and a final MIS 2 advance before ~17.7-17.6 cal ka BP (advance D) based on minimum deglacial ¹⁴C ages.

Kaplan et al. (2008) further constrained the Magallanes lobe MIS 2 chronology with nine additional ^{10}Be dates. They dated the innermost ridges on Punta Paulo, which are part of advance D, to 19.3 \pm 0.6 ka (n = 2). On Península Juan Mazía, they dated the innermost moraine (advance C) to 17.3 \pm 2.9 (n = 1) and the outermost (advance C) to 20.3 \pm 1.3 ka (n = 3). Together with three

ages from McCulloch et al. (2005b), they dated the innermost major right lateral moraine (advance B) to 27.5 ± 1.1 ka (n = 4); we note that in the maps presented by McCulloch et al. (2005b), Kaplan et al. (2008), and Soteres et al. (2020), this right lateral moraine appears to be part of the same dated moraine system that curves around Península Juan Mazía (Fig. 2A), so 27.5 ± 1.1 ka appears to be incongruously old. Farther northeast, on Primera Angostura, Kaplan et al. (2007) also dated four boulders with the 10 Be method to 24.3 ± 1.8 , 24.7 ± 3.1 , 26.6 ± 3.0 , 36.0 ± 4.0 ka (Fig. 2A).

Just south of the Magallanes lobe, Darvill et al. (2015) applied exposure dating to depth profiles in outwash deposited by the Bahía Inútil-San Sebastián glacier lobe. They found that deposits previously thought to be MIS 10 and 12 in age were likely deposited during the last glacial cycle, which they inferred to be during MIS 3.

Bog and lake sediments have provided additional insight into the history and deglaciation of the Magallanes lobe. Laminated glaciolacustrine sediments found capping glacial deposits provide evidence that a proglacial lake occupied the strait (McCulloch and Bentley, 1998), which McCulloch et al. (2005a) suggested was dammed by a large ice sheet-sized readvance during the Antarctic Cold Reversal. However, Hall et al. (2013) presented minimumlimiting radiocarbon dates of the last time glaciers occupied the fjords of Cordillera Darwin and showed that glaciers had retreated and remained in the cordillera by 16.8 \pm 0.35 cal ka BP. Based on seismic stratigraphy and swath bathymetry, Fernández et al. (2017) found evidence that the Magallanes ice was grounded in the shallow terminus area at least for part of the last glacial cycle. These authors also found evidence for morainal banks that they interpreted to correlate with the innermost LGM limit. They observed these morainal banks only in the shallower, low gradient areas, potentially reflecting a rapid retreat from this innermost glacial margin on Punta Paulo (Fig. 2A) through the deeper troughs of the strait. Fernández et al. (2017) also found no evidence for an extensive ice sheet expansion during the Antarctic Cold Reversal.

3.2. Southern South America and MIS 4

In general, MIS 4 is thought to have been a less extreme glaciation globally than MIS 2. For example, benthic $\delta^{18}O$ MIS 4 values increase by ~80% of MIS 2 values in the LR04 stack (Fig. 8E; Lisiecki and Raymo, 2005) relative to the Holocene. Similarly, dust flux from

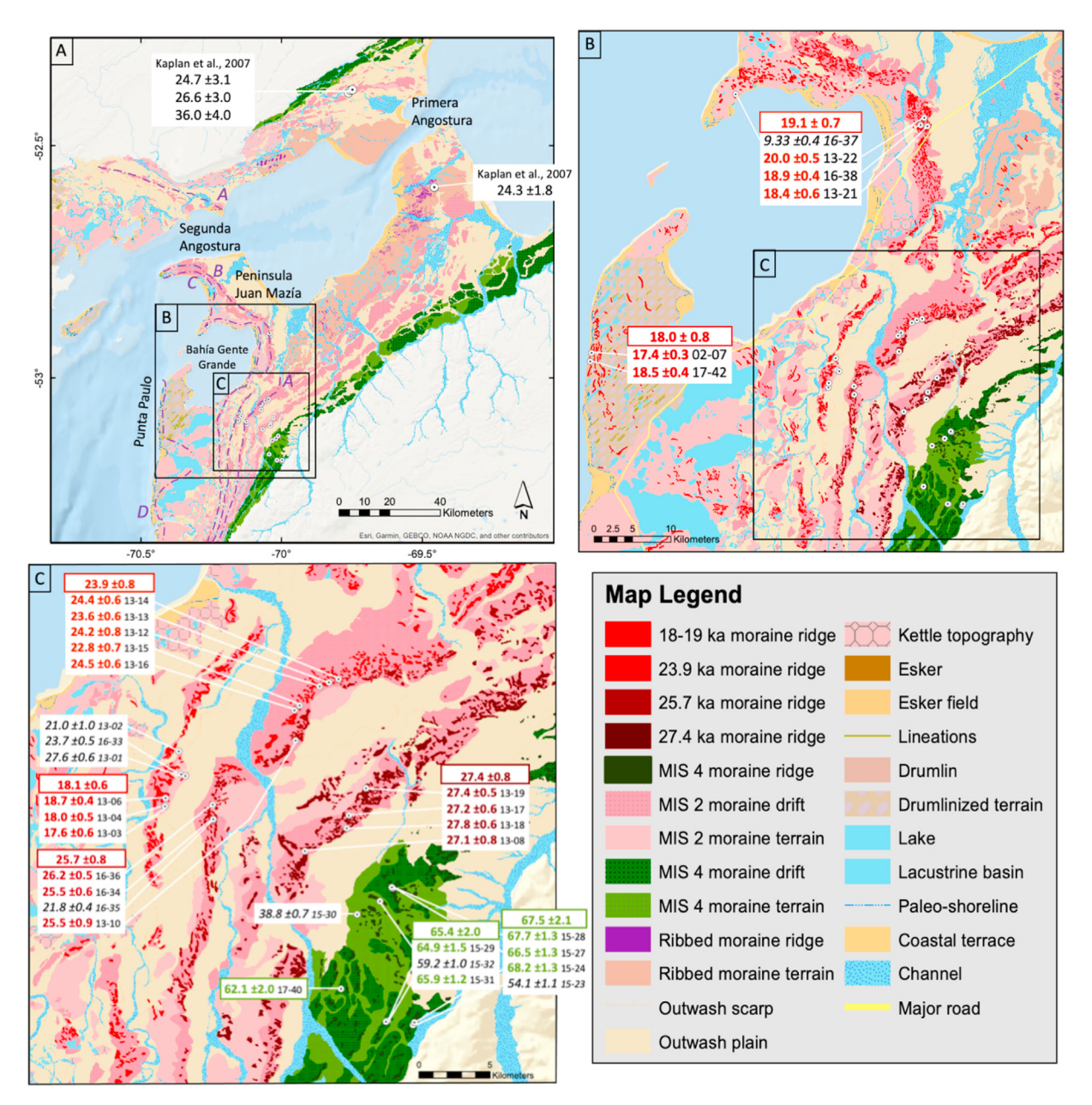


Fig. 2. Geomorphic map. Adapted from Soteres et al. (2020) with newly mapped moraine crests and 34 new ¹⁰Be ages. A. Purple dashed lines with italic alphabetical labels demarcate the approximate limits of advances A-D described in past work. B—C. Within the white boxes, mean moraine ages are shown on top (±the standard error of the mean, including the 3% propagated production rate error). Individual samples are shown with their internal error and sample name in black. Ages in black italic are excluded from the mean ages. See Fig. 3 for a detailed view of the MIS 4 moraine. Not all of the glacial landforms mapped are visible here, refer to Soteres et al. (2020) to see the full geomorphic map. (For interpretation of the references to color in this figure legend, the reader is referred to the Web version of this article.)

EPICA Dome C (Lambert et al., 2012) during the peak of MIS 4 is about ~75% of that of MIS 2 relative to Holocene values. In fact, the "penultimate" glacial period, or glaciation, is commonly understood as MIS 6 (e.g., Jouzel et al., 1993; Jakobsson et al., 2016), implying that MIS 4 was not a full glaciation.

In South America, little is known about MIS 4. In the Chilean Lake District at 40° S, Heusser et al. (2000) studied a bog core from Fundo Nueva Braunau that goes back to 60,000-70,000 14 C yr BP, based on an extrapolated radiocarbon age model from the upper

portion of the record to its base, allowing them to infer that the basal section was deposited during MIS 4. The palynology from this site suggests that conditions during the putative MIS 4 and MIS 2 were colder and wetter than present, with climate similar to environments located ~10° of latitude farther south relative to modern, and interpreted the vegetation from these periods as Subantarctic Parkland. Also in the Lake District, at 42°S, Heusser and Heusser (2006) collected a core at Taiquemó that extends beyond the limit of radiocarbon dating and potentially into MIS 4.

They found the pollen assemblages at the base of the core to be indicative of stadial conditions, similar to modern climates much farther south in Tierra del Fuego.

4. Methods

4.1. Geomorphic mapping and ¹⁰Be cosmogenic exposure age dating

Our work was carried out in conjunction with Soteres et al. (2020) who developed a high-resolution glacial geomorphic map of the study area. Here, we build on their work by dividing the MIS 2 moraines into dated groups and mapping the individual crests (Fig. 2B and C) to understand the morphostratigraphic relationships among landforms. We also mapped the ice contact slopes within the MIS 4 moraine complex (Fig. 3). We build and improve on the prior chronologies of McCulloch et al. (2005b) and Kaplan et al. (2008) by (1) pairing our results with the new high resolution geomorphic map, (2) employing developments in the ¹⁰Be method (Schaefer et al., 2009) that allow us to produce higher precision dates, and perhaps most importantly, (3) obtaining a suite of new ¹⁰Be dates across a large swath of the right lateral moraines and associated frontal area, including the first from pre-LGM deposits (Fig. 3).

We collected moraine ridge-top boulders during field campaigns in 2013, 2015, and 2016. As these boulders rest on the surface, they likely were deposited at the end of the moraine building event, so we interpret the ages as most likely representing the end of the period of glacial stability. We also resampled and reanalyzed 6 boulders dated in prior studies to obtain more precise ages (Table 3). We gave sampling priority to tall boulders embedded on the crests of moraine ridges with the goal of minimizing the influence of geomorphic processes (e.g., denudation, meltwater erosion during deglaciation). We chiseled samples from the top ~2 cm of the boulders, away from fresh-looking and spallation surfaces. We measured the locations of samples from the 2013 and 2015 field seasons with a regular hand-held Garmin GPS, and for the 2016 field season with differential Trimble GPS and corrected the positions with measurements from the Punta Arenas Satellite Station run by the Swedish Space Corporation in order to record the elevation of our samples as precisely and accurately as possible. We sampled largely granitoids (granites, granodiorites, diorites), but also greywackes and sandstones when granitic boulders were not available.

We isolated ¹⁰Be at the Lamont-Doherty Cosmogenic Nuclide Laboratory using standard methods (e.g., Schaefer et al., 2009; Kaplan et al., 2011) and measured the samples at the Lawrence Livermore National Laboratory Center for Accelerator Mass Spectrometry (Table 1). Ratios were measured relative to the standard 07KNSTD3110, with $a^{10}Be/^{9}Be$ ratio of 2.85 \times 10 $^{-12}$ (Nishiizumi et al., 2007). We used version 3 of the CRONUS-Earth online calculator (Balco et al., 2008), along with a regional nuclide production rate developed at Lago Argentino, Patagonia (50°S; Kaplan et al., 2011), which is statistically indistinguishable from the other Southern Hemisphere mid-latitude production rate, from New Zealand (Putnam et al., 2010). We calculated the ages assuming a rock density of 2.65 g/cm³. We measured topographic shielding using a compass and clinometer (although shielding at this site is very low; the maximum shielding value produced an age difference of 17 years). We calculate the ages using the non-time-dependent scaling (St) from Stone et al. (2000), the time dependent scaling (Lm) of Stone/Lal (Lal, 1991; Stone, 2000), and the LSDn scaling of Lifton et al. (2014) based on modeled fluxes of cosmic-rays. We discuss ages calculated using the Lm scheme in the text, although the choice of scheme does not impact our main conclusions. We calculated mean ages for moraines and present them with the

standard error of the mean and 3% propagated production rate error (Kaplan et al., 2011). We recalculate all ¹⁰Be ages from prior publications using the same systematics.

We present the ages with no correction for erosion rather than applying a single poorly constrained rate to all of our data. First, erosion is likely quite variable between boulders. A far-maximum erosion rate of ~1.4 mm/kyr at Lago Buenos Aires was presented in Kaplan et al. (2005): however, the standard deviation of the value is greater than half of the erosion rate. Kaplan et al. (2005) assumed the erosion rate was a maximum because the sampled boulders were likely exhumed, an inference strongly supported by the subsequently much lower median rate of 0.2 mm/kyr obtained by Douglass et al. (2007). Second, we only collect samples that appear to be from original surfaces. We did find ventifact characteristics on the sides of some boulders, but top surfaces from which we specifically sampled were generally smooth and did not show substantial micro relief or evidence of erosion. Last, we note that the production rate we used to calculate our ages was derived empirically from boulders that likely experienced a similar erosion rate, as the calibration site is just 300 km to the north in a similar climate regime, so in this way perhaps erosion is already partially accounted for in at least the MIS 2 age calculation. For the above reasons, we discuss our ages calculated without an erosion correction. For each moraine group, we also note the maximum age without an erosion correction. For reference, applying an erosion rate of 0.2 mm/kyr (derived in Douglass et al., 2007) would increase the youngest MIS 2 ages by 0.3% (53 years), the oldest MIS 2 ages by 0.5% (124 years) and the MIS 4 ages on average by 1% (745 years). An erosion rate of ~1 mm/kyr (cf., the maximum rate in Kaplan et al., 2005) would increase the youngest MIS 2 ages by 1.5% (270 years), the oldest MIS 2 ages by 2.3% (633 years) and the MIS 4 ages on average by 6% (4 thousand years; still placing the moraine within MIS 4).

Lastly, to obtain a first-order estimate of climate anomalies relative to present for Estrecho de Magallanes, we reconstructed past glacier extent using the University of Maine Ice Sheet Model (UMISM) (Fastook and Prentice, 1994; Fastook et al., 2008). We carried out an initial set of sensitivity experiments driven by temperature and precipitation boundary conditions configured atop 1.2 km topography and bathymetry simulations. The model description and results are presented in the Supplementary Material.

5. Results

5.1. Chronology

Within our study area (Fig. 2C), moraines follow a rotated "C" shape, where in the southern sector the moraines are generally oriented N-S, and in the middle of the panel they curve towards the NE. The outermost moraine complex (depicted in green in Figs. 2 and 3) has an overall width similar to the width of ~two MIS 2 moraines. It contains a series of moraine drifts and channels that are roughly parallel to the more interior (red-colored) moraines. These likely represent separate moments of glacier stability that we infer are reflected in our chronology. The ages within the moraine are in morphostratigraphic sequence, where the outermost dated ridge produced an average age of 67.5 ± 2.1 ka (n = 3), followed by 65.4 ± 2.0 ka (n = 2), and 62.1 ± 2.0 ka (n = 1) (Table 2). All ages on the 67.5 \pm 2.1 ka moraine ridges are older than all ages on the 65.4 ± 2.0 ka moraine ridges, with the exception of SM-15-32 and SM-15-23 which we consider outliers as their ages are more than 2σ younger than taller, nearby boulders (within 130 m) located in the same morphostratigraphic position (Fig. 4); we assume erosion/ denudation may have affected their ages (see section 5.3 for further

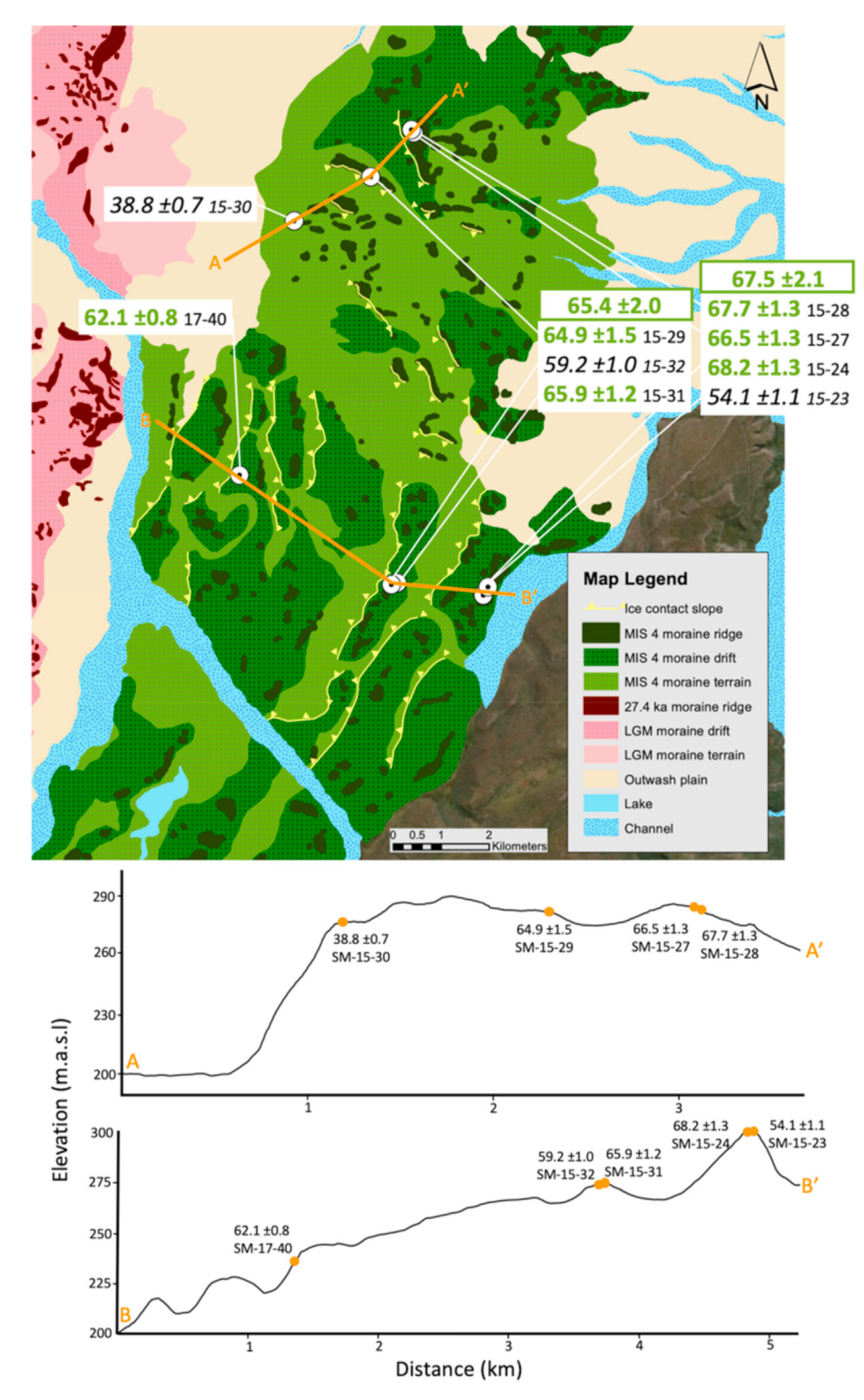


Fig. 3. Additional focus on the MIS 4 moraine and morphostratigraphic context of the 10 Be ages. To illustrate the relationships between the dated boulders, the lower panels show elevation profiles across the moraine along orange lines A-A' and B-B' visible in the top panel; profile shows distance from younger to older part of the moraine. Also note the slight change in trend of the ice contact slopes, which appears to mirror the general trend of the right lateral moraine systems shown on prior Fig. 2B. All ages are in stratigraphic order except for SM-15-32 and SM-15-32 (which may be younger than the moraine due to the low boulder height and moraine surface deflation, see Fig. 4). The MIS 4 moraine has a sequence of moraine ridges and channels that represent separate periods of glacier stability within MIS 4. We propose that the outer ages represent an older advance at 67.5 ± 2.1 ka (n = 3), followed by an advance at 65.4 ± 2.0 ka (n = 2), and potentially at 62.1 ± 2.0 ka (n = 1) and 38.8 ± 0.7 ka (n = 1). Note two additional crests along the B-B' profile remain undated. (For interpretation of the references to color in this figure legend, the reader is referred to the Web version of this article.)

Table 1 Geographic and 10 Be analytical data. Analytical data for 10 Be age calculation, sorted into moraine groups with italics showing samples that are excluded from the moraine means. Boron-corrected 10 Be/ 9 Be values were measured against the 07KNSTD AMS standard with a reported 10 Be/ 9 Be value of 2.85 × 10 12 (Nishiizumi et al., 2007; 10 Be half-life = 1.36 Myr). 1 σ analytical or internal AMS uncertainties are shown. Density = 2.65 g/cm 3 . 10 Be concentrations are corrected for 10 Be in process blanks run with each sample batch. Carrier concentrations in ppm as follows, with the 10 Be/ 9 Be ratios measured in the process blanks in each sample batch: (a) 1038.68, 7.678 × 10 -16, (b) 1047.17, 4.623 × 10 -16, (c) 1027.73, 1.137 × 10 -16, (d) 1029.87, 6.783 × 10 -16 and 1.612 × 10 -15, (e) 1031.58, 1.90095 × 10 -16, (f) 1031.96, 6.732 × 10 -16, (g) 1028.2, 8.7609 × 10 -16.

Sample	CAMS no.	Latitude	Longitude	Elevation	Boulder ht.	Thickness	Shielding	Quartz wt	⁹ Be Carrier	¹⁰ Be/ ⁹ Be	¹⁰ Be Concentration
Moraine gr	roup	(DD)	(DD)	(m.a.s.l.)	(cm)	(cm)		(g)	(g)	(10 ⁻¹⁴)	(10 ⁴ atoms g ⁻¹)
18.0 ka mc	oraine-Punto	a Paulo									
SM-17-42	BE47283	-53.0746	-70.4325	32	52	1.1	1.0000	11.2673	0.1806 ^g	7.7030 ± 0.1527	8.388 ± 0.17
SM-02-07	BE47282	-53.0689	-70.4311	31	94	1.3	1.0000	15.4153	0.1812 ^g	9.7696 ± 0.1821	7.821 ± 0.15
18.1 ka ma	oraine - mai	n sequence									
SM-13-03	BE38353	-53.0929	-70.1553	115	70	1.0	1.0000	7.0031	0.1818 ^a	4.8887 ± 0.1772	8.672 ± 0.32
SM-13-04	BE38354	-53.0928	-70.1549	118	105	1.1	0.9941	7.0525	0.1810 ^a	5.0240 ± 0.1265	8.819 ± 0.22
SM-13-06	BE41380	-53.0896	-70.1544	129	85	1.5	1.0000	13.0157	0.1821 ^c	9.6972 ± 0.2180	9.308 ± 0.21
Resampled	l boulders										
SM-13-02	BE41959	-53.0721	-70.1463	81	90	3.2	0.9998	4.6646	0.1810^{e}	3.6841 ± 0.1747	9.811 ± 0.47
SM-13-01	BE41379	-53.0813	-70.1421	120	140	1.1	1.0000	13.5718	0.1820^{c}	14.880 ± 0.3175	$13.681 \pm 0.29 $
SM-16-33	BE41666	-53.0807	-70.1448	99	90	0.6	0.9998	10.9871	0.1810^{d}	10.268 ± 0.1978	11.553 ± 0.22
19.1 ka mo	oraine - Juan	ı Mazia									
SM-13-22	BE41385	-52.9035	-70.0431	58	180	3.4	1.0000	13.4947	0.1820 ^c	9.8567 ± 0.2289	9.121 ± 0.21
		-52.9087	-70.0474	58		1.6	1.0000	9.7871	0.1830 ^e	6.7952 ± 0.1295	8.712 ± 0.17
SM-13-21		-52.9094	-70.0393	53	40	1.5	0.9988	13.4628	0.1817 ^c	9.1407 ± 0.2732	8.464 ± 0.25
SM-16-37		-52.8869	-70.2627	19	99	0.9	1.0000	5.0376	0.1820^{e}	1.6818 ± 0.0632	4.147 ± 0.16
23.9 ka mo											
SM-13-15		-53.0545	-70.0699	143	85	1.2	0.9997	7.0247	0.1823 ^a	6.4755 ± 0.1981	11.528 ± 0.35
SM-13-13	BE38356	-53.0459	-70.0515	152	100	0.9	1.0000	7.0146	0.1818 ^a	6.7784 ± 0.1813	12.058 ± 0.32
SM-13-12		-53.0474	-70.0574	156	98	1.1	1.0000	7.0864	0.1820 ^a	7.0282 ± 0.2193	12.387 ± 0.39
SM-13-14		-53.0447	-70.0455	146	70	1.1	1.0000	8.9051	0.1807 ^c	8.8983 ± 0.2163	12.387 ± 0.30
SM-13-16	BE38358	-53.0565	-70.0733	145	75	1.6	1.0000	7.0287	0.1828 ^a	6.9384 ± 0.1748	12.390 ± 0.31
25.7 ka mo										_	_
SM-16-34	BE41960	-53.0980	-70.1245	166	215	2.0	1.0000	15.1915	0.1821 ^e	15.869 ± 0.3993	13.100 ± 0.33
SM-13-10	BE41661	-53.0680	-70.0725	141	70	1.1	1.0000	10.5780	0.1803 ^d	11.041 ± 0.4059	12.873 ± 0.47
SM-16-36	BE41962	-53.0922	-70.1248	159	60	1.7	1.0000	11.3695	0.1830 ^e	12.161 ± 0.2139	13.438 ± 0.24
SM-16-35	BE41961	-53.0981	-70.1245	168	42	1.4	1.0000	11.4369	0.1820^{e}	10.310 ± 0.2096	11.291 ± 0.23
27.4 ka mo	oraine										
SM-13-08	BE41381	-53.1100	-70.0667	213	115	1.0	1.0000	7.3754	0.1828 ^c	8.6379 ± 0.2454	14.687 ± 0.42
SM-13-17	BE38359	-53.0963	-70.0389	183	110	0.9	0.9994	7.0336	0.1823 ^a	8.0470 ± 0.1731	14.342 ± 0.31
SM-13-19	BE41383	-53.0861	-70.0282	169	90	1.3	1.0000	8.6821	0.1814 ^c	9.9276 ± 0.1874	14.232 ± 0.27
SM-13-18	BE38360	-53.1014	-70.0404	199	180	1.1	0.9994	7.0113	0.1826 ^a	8.2907 ± 0.1852	14.852 ± 0.33
66.7 ka mo	oraine										
SM-15-29	BE40569	-53.1288	-70.0194	279	37	1.3	1.0000	5.0182	0.1806 ^b	14.823 ± 0.3354	37.219 ± 0.84
SM-15-31	BE41665	-53.1745	-70.0155	272	110	1.0	0.9999	8.2588	0.1812 ^d	24.999 ± 0.4305	37.652 ± 0.65
SM-15-27	BE41668	-53.1239	-70.0114	281	42	2.7	1.0000	21.1275	0.1810 ^d	64.217 ± 1.2134	37.752 ± 0.71
SM-15-28	BE41663	-53.1235	-70.0119	282	89	1.6	1.0000	8.8518	0.1818 ^d	27.540 ± 0.5371	38.838 ± 0.76
SM-15-24	BE40568	-53.1748	-69.9975	308	100	1.5	1.0000	7.0989	0.1807 ^b	22.593 ± 0.4208	40.169 ± 0.75
SM-15-30	BE41664	-53.1338	-70.0338	279	77	2.4	1.0000	8.7304	0.1820^{d}	15.515 ± 0.2586	22.154 ± 0.37
SM-15-23	BE41662	-53.1757	-69.9984	307	25	1.4	0.9998	8.3678	0.1820^{d}	21.416 ± 0.4173	31.891 ± 0.62
SM-15-32	BE41669	-53.1743	-70.0145	275	56	1.4	0.9999	30.7086	0.1820^{d}	83.199 ± 1.3482	33.820 ± 0.55
SM-17-40	BE43870	-53.1623	-70.0440	233	90	1.3	1.0000	19.6018	0.1420^{f}	68.640 ± 0.8447	34.142 ± 0.42
Previously	published, r									Originally published in:	
SM-02-07		-53.072	-70.436	31	90	0.5	1	26.241		Kaplan et al. (2008)	99.420 ± 6.4
SM-02-08		-53.069	-70.431	33	50	0.8	1	24.291		Kaplan et al. (2008)	100.70 ± 24
SM-02-09		-52.917	-70.038	49	35	0.9	1	8.822		Kaplan et al. (2008)	111.10 ± 12
SM-02-11		-52.909	-70.039	42	35	1.5	1	33.05		Kaplan et al. (2008)	113.36 ± 6.8
SM-02-12		-52.904	-70.043	45	163	3	1	13.634		Kaplan et al. (2008)	93.18 ± 8.4
SM-02-14		-52.934	-70.062	37	30	0.5	1	6.058		Kaplan et al. (2008)	89.930 ± 15
BGGC3		-53.083	-70.144	100	100	3	0.96	15.17		Kaplan et al. (2008)	147.18 ± 6.0
BGGC1		-53.071	-70.146	82	100	4	0.96	38.612		McCulloch et al. (2005)	148.98 ± 8.5
		-53.083	-70.144	100	200	4	0.96	52.002		McCulloch et al. (2005)	145.38 ± 12
BGGC2					200	4		22.977		McCulloch et al. (2005)	

discussion). The two groups of moraine ages are more than 2 SEM apart, although we note they are more than 1 but less than 2 standard deviations apart and so should only be cautiously distinguished. The innermost lower ridge of this moraine yielded an age of 38.8 \pm 0.7 ka (n = 1) (Figs. 2 and 3), albeit we only found one quartz-bearing boulder on this landform and hence the result needs to be replicated to determine if it accurately represents the crest age.

For the entire sequence, we calculate an average age of 66.7 ± 2.1 ka. This single mean age is based on 5 samples (4 excluded) with a

maximum age of 68.2 ± 1.3 ka (Figs. 2, 3 and 6, Table 2). While the ages 62.1 ± 0.8 and 38.8 ± 0.7 ka are in stratigraphic order, they are not included in a single mean age given they are statistically different from the mean (without the propagated production rate error) at two standard deviations and may have been impacted by geomorphic processes. Most importantly, the range of ages and the means place the deposition of the moraine complex squarely within MIS 4 regardless of uncertainties (Fig. 8A). All of the ages calculated using all three scaling schemes date to MIS 4 except for the two youngest outliers (Table 2). When calculated using an

Table 2

10 Be ages. 10 Be ages (ka) calculated using the non-time-dependent scaling (St) from Stone et al. (2000), the time dependent scaling (Lm) of Stone/Lal (Lal, 1991; Stone, 2000), and the LSDn scaling of Lifton et al. (2014). Mean moraine ages (shown in bold) exclude samples in italics, and are shown with the standard error of the mean and the propagated 3% error of the production rate (Kaplan et al., 2011). Samples were run at CAMS with the 07KNSTD standard but previously published samples were run at ETH using the standard S555, except for BGGC3 which was run at SUERC with the standard NIST_3000. See Table 3 for the previously published boulder ages calculated using our higher precision location data. No correction for snow cover or erosion was made to these data. The effect of applying a reasonable erosion rate is discussed in the text.

Moraine group	Sample	Age (St)	Age (Lm)	Age (LSDn)
	•	(ka)	(ka)	(ka)
18.0 ka moraine -Punta Paulo	SM-17-42	18.9 ± 0.4	18.5 ± 0.4	18.0 ± 0.4
	SM-02-07	17.8 ± 0.3	17.4 ± 0.3	16.9 ± 0.3
	Mean \pm SEM and PR error	$\textbf{18.4} \pm \textbf{0.8}$	$\textbf{18.0} \pm \textbf{0.8}$	17.4 ± 0.7
18.1 ka moraine -main sequence	SM-13-03	18.0 ± 0.7	17.6 ± 0.6	17.1 ± 0.6
	SM-13-04	18.3 ± 0.5	18.0 ± 0.5	17.5 ± 0.4
	SM-13-06 Mean \pm SEM and PR error	19.1 ± 0.4 18.5 ± 0.6	18.7 ± 0.4 18.1 ± 0.6	18.2 ± 0.4 17.6 \pm 0.6
Resampled boulders	SM-13-02	21.4 ± 1.0	21.0 ± 1.0	20.3 ± 1.0
Resumpled bodiders	SM-13-02 SM-13-01	28.3 ± 0.6	27.6 ± 0.6	26.7 ± 0.6
	SM-16-33	24.3 ± 0.5	23.7 ± 0.5	22.9 ± 0.4
19.1 ka moraine - Juan Mazía	SM-13-22	20.4 ± 0.5	20.0 ± 0.5	19.4 ± 0.5
	SM-16-38	19.2 ± 0.4	18.9 ± 0.4	18.3 ± 0.4
	SM-13-21	18.8 ± 0.6	18.4 ± 0.6	17.9 ± 0.5
	SM-16-37	9.5 ± 0.4	9.33 ± 0.4	9.1 ± 0.4
	Mean ± SEM and PR error	19.5 ± 0.8	19.1 ± 0.7	18.5 ± 0.7
23.9 ka moraine	SM-13-15	23.3 ± 0.7	22.8 ± 0.7	22.1 ± 0.7
	SM-13-13	24.1 ± 0.7	23.6 ± 0.6	22.8 ± 0.6
	SM-13-12	24.7 ± 0.8	24.2 ± 0.8	23.4 ± 0.7
	SM-13-14	25.0 ± 0.6	24.4 ± 0.6	23.6 ± 0.6
	SM-13-16 Mean \pm SEM and PR error	25.1 ± 0.6 24.4 ± 0.8	24.5 ± 0.6 23.9 ± 0.8	23.7 ± 0.6 23.1 \pm 0.8
25.7 ka moraine	SM-16-34	26.0 ± 0.7	25.5 ± 0.6	24.6 ± 0.6
25.7 Ka Hioranic	SM-13-10	26.0 ± 0.7 26.1 ± 1.0	25.5 ± 0.0 25.5 ± 0.9	24.0 ± 0.0 24.7 ± 0.9
	SM-16-36	26.8 ± 0.5	26.2 ± 0.5	25.4 ± 0.5
	SM-16-35	22.3 ± 0.5	20.2 ± 0.5 21.8 ± 0.4	23.4 ± 0.3 21.2 ± 0.4
	Mean \pm SEM and PR error	26.3 ± 0.8	25.7 ± 0.8	24.9 ± 0.8
27.4 ka moraine	SM-13-08	27.7 ± 0.8	27.1 ± 0.8	26.2 ± 0.8
	SM-13-17	27.8 ± 0.6	27.2 ± 0.6	26.3 ± 0.6
	SM-13-19	28.1 ± 0.5	27.4 ± 0.5	26.5 ± 0.5
	SM-13-18	28.4 ± 0.6	27.8 ± 0.6	26.9 ± 0.6
	Mean ± SEM and PR error	28.0 ± 0.9	27.4 ± 0.8	26.5 ± 0.8
66.7 ka moraine	SM-15-29	66.8 ± 1.5	64.9 ± 1.5	62.9 ± 1.4
	SM-15-31	67.8 ± 1.2	65.9 ± 1.2	63.8 ± 1.1
	SM-15-27	68.4 ± 1.3	66.5 ± 1.3	64.4 ± 1.2
	SM-15-28	69.7 ± 1.4	67.7 ± 1.3	65.6 ± 1.3
	SM-15-24 SM-15-30	70.2 ± 1.3 39.8 ± 0.7	68.2 ± 1.3 38.8 ± 0.7	66.0 ± 1.3
	SM-15-23		54.1 ± 1.1	37.5 ± 0.6
	SM-15-32	55.6 ± 1.1 60.8 ± 1.0	59.2 ± 1.0	52.4 ± 1.0 57.4 ± 0.9
	SM-17-40	63.9 ± 0.8	62.1 ± 0.8	60.2 ± 0.8
	Mean ± SEM and PR error	68.6 ± 2.5	66.7 ± 2.1	64.5 ± 2.3
Originially published in Kaplan et al. (2008)	SM-02-07	20.4 ± 1.3	20.0 ± 1.3	19.3 ± 1.2
	SM-02-08	20.7 ± 4.9	20.2 ± 4.8	19.6 ± 4.7
	SM-02-09	22.5 ± 2.4	22.0 ± 2.4	21.3 ± 2.3
	SM-02-11	23.2 ± 1.4	22.7 ± 1.4	21.9 ± 1.3
	SM-02-12	19.2 ± 1.7	18.9 ± 1.7	18.3 ± 1.6
	SM-02-14	18.3 ± 3.1	18.0 ± 3.0	17.4 ± 2.9
	BGGC3	30.6 ± 1.3	29.9 ± 1.2	28.8 ± 1.2
Originially published in McCulloch et al. (2005)	BGGC1	31.1 ± 1.8	30.4 ± 1.7	29.3 ± 1.7
	BGGC2	29.8 ± 2.6	29.1 ± 2.5	28.1 ± 2.4
	BGGC4	28.5 ± 1.0	27.9 ± 1.0	26.8 ± 1.0

erosion rate of ~1 mm/kyr (cf., the maximum erosion rate from Kaplan et al., 2005), the outermost moraine still lies within MIS 4. Another possible interpretation of the morphostratigraphic order of the pre-LGM (mapped in green) dataset is that this sequence of moraine crests was deposited within a shorter time span than the ages suggest, but the inboard crests experienced higher erosion

rates than the outboard crests, as they were more proximal to the glacier margin during the subsequent MIS 2 glaciation.

The next inboard moraine has much finer scale crests preserved when compared with the MIS 4 moraine, and represents the most extensive MIS 2 glacial advance in the study area (mapped in red on



Fig. 4. Five sets of sample pairs. In each pair, the taller boulder is also the older boulder. We note that in the bottom two pairs, the ages are indistinguishable within error. Red dotted lines represent moraine crests. (For interpretation of the references to color in this figure legend, the reader is referred to the Web version of this article.)

Fig. 2). We date this moraine to 27.4 ± 0.8 ka (n = 4; Fig. 2b). Ages are particularly internally consistent on this moraine, ranging from 27.1 ± 0.8 to 27.8 ± 0.6 ka. Near the terminal margin to the northeast, this moraine bifurcates into 2-3 drifts separated by outwash and meltwater channels.

The next moraine complex is composed of two sets of ridges. Three samples from boulders on the outer set of moraine crests yielded ages of 25.5 ± 0.9 , 25.5 ± 0.6 and 26.2 ± 0.5 ka (mean age of 25.7 ± 0.8 ka; sample 16-35 was excluded as it is an outlier (Figs. 2 and 4)). On the same drift, we date the next advance to 23.9 ± 0.8 ka (n = 5), ranging from 24.5 ± 0.6 ka to 22.8 ± 0.7 ka. While these two dated advances occupy the same moraine unit, this moraine contains multiple sets of moraine crests, where the average elevation of the samples on the outer crests is ~10 m higher than on the inner crest. About 10 km to the northeast, the moraine divides into at least three units, where the innermost margin curves towards Península Juan Mazía and the outer margins terminate at Primera Angostura.

Next, we collected four samples from a moraine complex on Península Juan Mazía. The samples produced a mean age of 19.1 ± 0.7 ka (n=3) with a range from 20.0 ± 0.5 to 18.4 ± 0.6 ka. We excluded sample SM-16-37 because it is anomalously young $(9.3 \pm 0.4$ ka). It has an elevation of 19 m.a.s.l. and is just north of paleo-shorelines at ~10 m.a.s.l., making it possible that this area was affected by a post-glacial lake, or nearby human disturbance noted while collecting this sample. Towards the south, we dated another portion of the right lateral moraine complex that appears

to terminate on Península Juan Mazía. This moraine is much narrower than the rest of the sequence, and appears to have been affected by meltwater on all sides, but it has sharp, well-preserved crests in the region that we sampled (Fig. 5). This is the innermost major moraine in the study area and we date it to 18.1 ± 0.6 ka (n=3), with a range from 18.7 ± 0.4 to 17.6 ± 0.6 ka. The 19.1 ± 0.7 ka and 18.1 ± 0.6 ka moraines may be part of the same overall moraine complex with multiple advances represented in one unit. Their stratigraphic relationship is unclear and they are statistically indistinguishable so we suggest that they were deposited during the same overall event.

Finally, on Punta Paulo we mapped in detail a series of small recessional moraine crests deposited over drumlinized terrain (Fig. 2B; these were also mapped previously by Benn and Clapperton (2000), Bentley et al. (2005), Lovell et al. (2011), and Darvill et al. (2014). These moraine crests vary greatly from the rest of the moraine complexes that we dated which sit prominently above the surrounding topography (>~30 m). The narrow moraine crests deposited over drumlinized terrain on Punta Paulo rise only a few meters above the surrounding terrain and are of a similar scale to the drumlins on which they were deposited but with opposing orientation. Two samples on boulders atop these ridges yielded ages of 17.4 \pm 0.3 and 18.5 \pm 0.4 ka (mean: 18.0 \pm 0.8 ka); the former age is on a resampled boulder from Kaplan et al. (2008) (Table 3). The average sample elevation is just 32 m.a.s.l., whereas the average sample elevation of the 18.1 \pm 0.6 ka moraine, ~20 km directly to the east, is 121 m.a.s.l. So while they are statistically

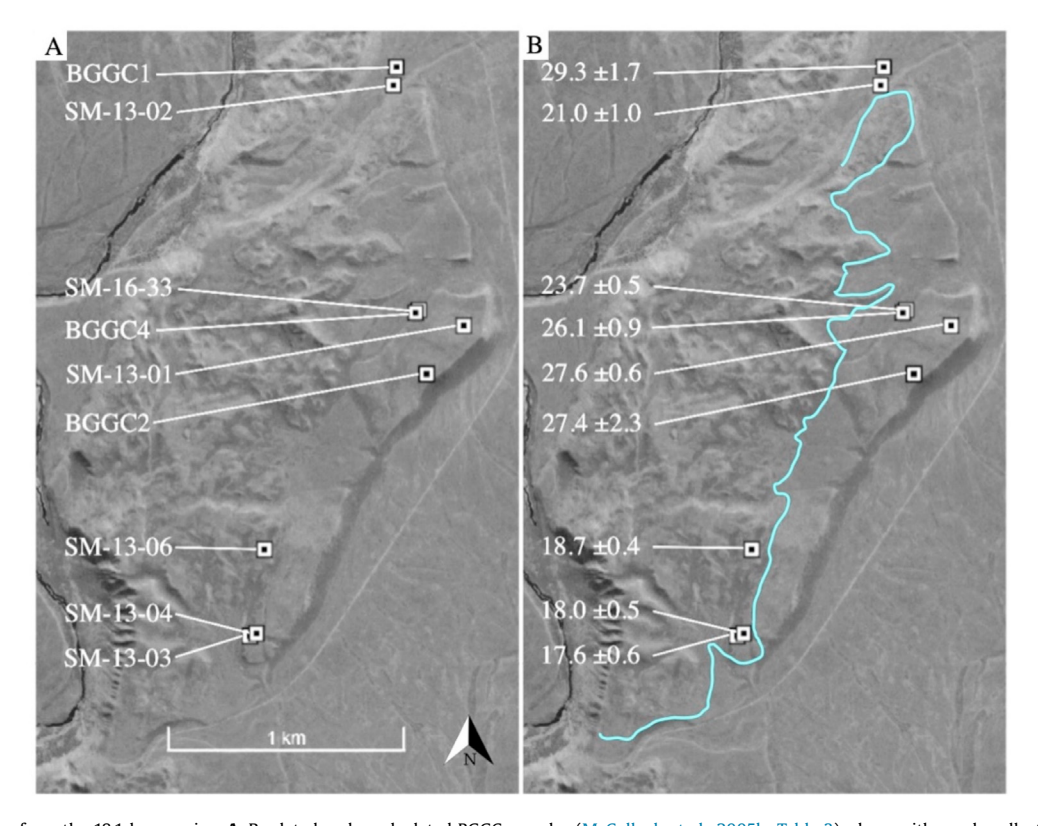


Fig. 5. Sample locations from the 18.1 ka moraine. **A.** Re-dated and recalculated BGGC samples (McCulloch et al., 2005b; Table 3), along with newly collected samples (the three southernmost samples). BGGC samples are plotted at the latitudes and longitudes given in McCulloch et al. (2005b), but we note that we were unable to locate samples BGGC2 and BGGC3 which have the same location data as one another. Based on our field observations and personal communication with C. Fogwill, we matched our re-collected sample sites with those of McCulloch et al. (2005b) in Table 3. The closest boulder to the position given for BGGC2 and BGGC3 was at our site SM-13-01 and a photo of this same boulder being sampled appears in Fig. 2 of McCulloch et al. (2005b); based on the available information, we concluded that BGGC2 and SM-13-01 are likely from the same boulder. **B.** Sample ages and the boundary between moraine and fluvial topography is represented as a blue line. We propose that while the glacier was sitting at the 18.1 ± 0.6 ka moraine margin, inside the blue line, glacio-fluvial outwash uncovered older underlying sediments just beyond the margin, which is reflected in the scatter and older ages of the BGGC samples. In addition, samples BGCC1 (SM-13-02) and BGGC4 (SM-16-33) are located in a gulley cut on the side of the crest. (For interpretation of the references to color in this figure legend, the reader is referred to the Web version of this article.)

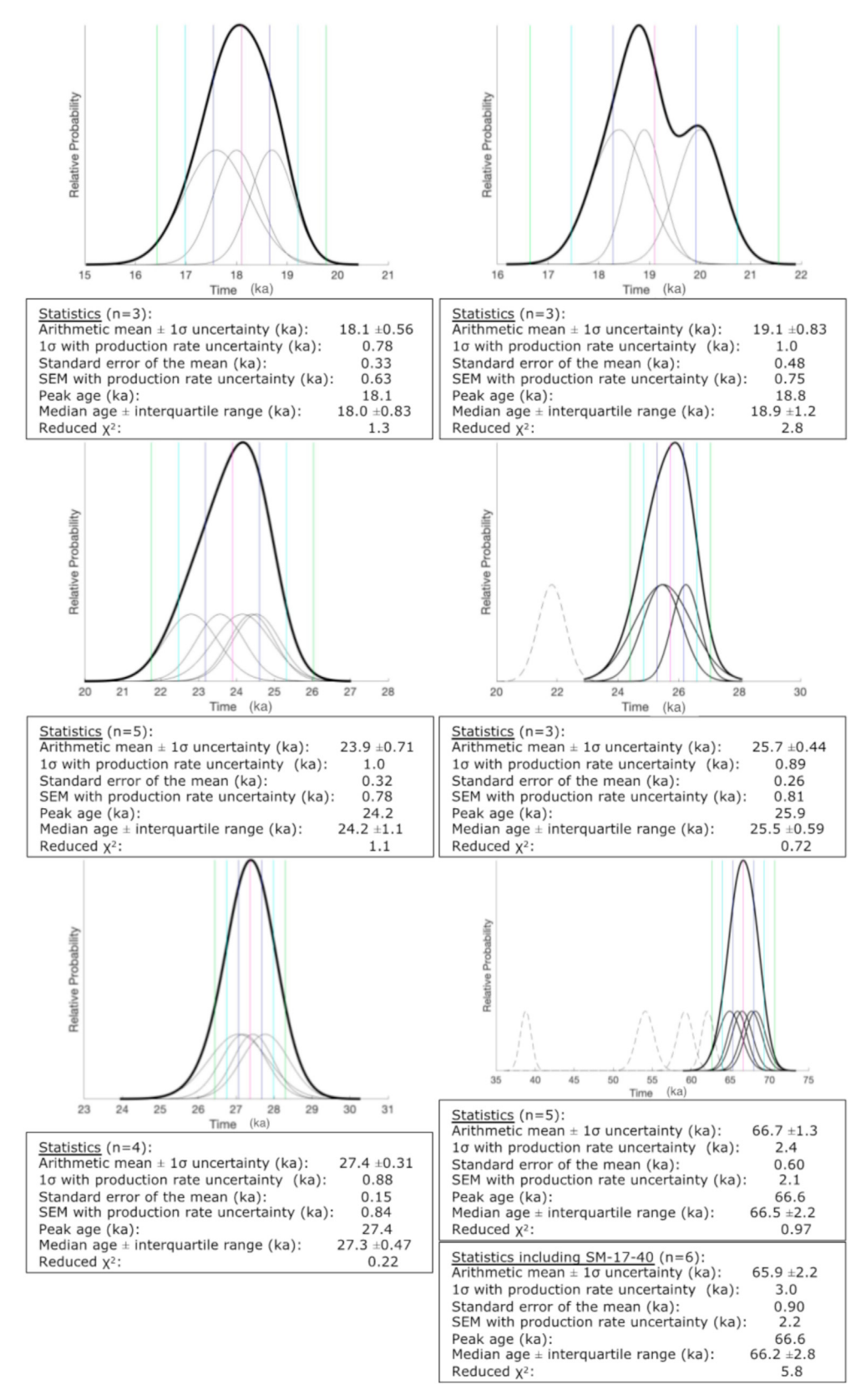


Fig. 6. 10 Be ages and descriptive statistics for the moraine sequence at Estrecho de Magallanes. Thin black lines are normal kernel density estimates of individual samples with their 1σ internal error. Thick lines are the sums of the individual curves. Dashed curves are excluded from the summed curve (n=1 for MIS 2, and n=4 for pre-LGM moraines). Pink lines are the mean ages, blue, cyan and green lines are the 1, 2, and 3 σ bounds respectively. This sequence, along with the more detailed \sim 65.4 and \sim 67.5 ka normal kernel density estimates, are all plotted in Fig. 8A. In the text we reference the arithmetic mean age and the standard error of the mean (SEM) with a 3% propagated production rate uncertainty (Table 2). (For interpretation of the references to color in this figure legend, the reader is referred to the Web version of this article.)

Table 3
Resampled boulders. All previously published ages, which were measured at ETH, were recalculated the same way in this study (V3 of the Balco et al. (2008) calculator, Kaplan et al. (2011) production rate, Lm scaling) using the location and shielding values we collected. Only one sample, *in italics*, gave an age beyond 2σ of the prior age.

This	study			Age difference (ka)	
Sample	Age (ka)	Formerly known as:	Age (ka)	First published by:	
SM-13-02	21.0 ± 1.0	BGGC1	29.3 ± 1.7	McCulloch et al. (2005)	-8.3
SM-13-01	27.6 ± 0.6	BGGC2	27.4 ± 2.3	McCulloch et al. (2005)	0.2
SM-16-33	23.7 ± 0.5	BGGC4	26.1 ± 0.95	McCulloch et al. (2005)	-2.4
SM-02-07	17.4 ± 0.3	SM-02-07	20.1 ± 1.3	Kaplan et al. (2008)	-2.6
SM-13-21	18.4 ± 0.6	SM-02-11	22.5 ± 1.4	Kaplan et al. (2008)	-4.1
SM-13-22	20.0 ± 0.5	SM-02-12	18.6 ± 1.7	Kaplan et al. (2008)	1.4

indistinguishable in age, they are geomorphically distinct. As these crests may be recessional features (Soteres et al., 2020), it is to be expected that they date closely to the next outboard neighboring moraine, as we assume boulders on the surface of the two moraines date the last moment that the glacier sat at these margins.

5.2. Resampled boulders: results and interpretations

All but one of the six resampled boulders afforded ages that are statistically indistinguishable within two standard deviations from previous measurements but analytical uncertainties (internal errors) are reduced now to <5% (Table 3) or multi-century resolution (e.g., SM-02-07). The differences in nuclide concentrations are what we expect given adjustments for respective AMS standardizations used at ETH and CAMS. Of note, the three ages from the previously sampled boulders are older (~30-28 ka) than the new ¹⁰Be-dated moraine they appear to be associated with (18.1 \pm 0.6 ka), with one age even older than the outboard moraine. This caused us to reevaluate the setting during our mapping of the landform, as we show in Fig. 5. Given the satellite imagery now available and the spread of the data, we assume that the three ages from McCulloch et al. (2005b), remeasured in this study, are part of an older deposit covered by a later advance, and were exhumed by glaciofluvial meltwater associated with the 18.1 ka margin. Specifically, Fig. 5 shows SM-13-01 (BGGC2) and SM-16-33 (BGGC4) are in an area with a smoother texture, similar to fluvial topography, lacking the moraine crest texture of the 18.1 ka moraine just inboard. Furthermore, the sample site of SM-13-02 (BGGC1) is along a channel cut into the side of the crest, and may have been originally deposited in what is now subsurface till.

5.3. Boulder height versus exposure age: results and interpretations

We collected five pairs of samples from boulders that are in

close proximity to one another (usually within eyeshot) to explore whether boulder height or position (relative to the top of the moraine crest) correlate with exposure age. In every sample pair the taller boulder is older, regardless of its position on the moraine (Fig. 4), although we do note that for two pairs, the ages are statistically indistinguishable within uncertainty. We also plot the boulder height against exposure age (Fig. 7) and find that a linear model weakly explains the variance for the data ($R^2 = 0.09$); the relationship appears stronger for boulders shorter than 90 cm, where the slope is 0.001 (Fig. 7B), suggesting that for boulders below ~1 m, height may have a weak influence on apparent exposure age. We also note that in three of these pairs (SM-15-32, SM-16-35, and SM-15-27), the taller, older boulder is on the edge or side of the moraine crest, while the shorter, younger boulder is on top of the crest. This leads us to infer that given a choice between sampling a short boulder (<~1 m) on the crest of a moraine or a tall boulder on the slope, the shorter boulder may be more likely to give a younger apparent age, at least for moraines that are 20 ka and older.

As an exercise, we then used the five boulder pairs to evaluate the rate of moraine denudation. We reiterate that two of these pairs are indistinguishable within error. Each boulder pair has a younger, shorter and an older, taller boulder on the same landform right next to each other meaning they were likely deposited synchronously. We think the most plausible explanation for why the shorter boulders are uniformly younger is that they were originally covered, but moraine denudation exposed them sometime post-deposition. We use the age difference between the two boulders to calculate an average moraine denudation rate. This assumes erosion happened at a constant rate, while it seems more likely that erosion rates were episodic, higher during glaciation (e.g., during MIS 2 for the MIS 4 moraines) and since the 19th century as a result of domestic animal grazing. We add the calculated erosion to the height of the shorter boulder to get 54, 44, 69, 61, 73 cm of moraine

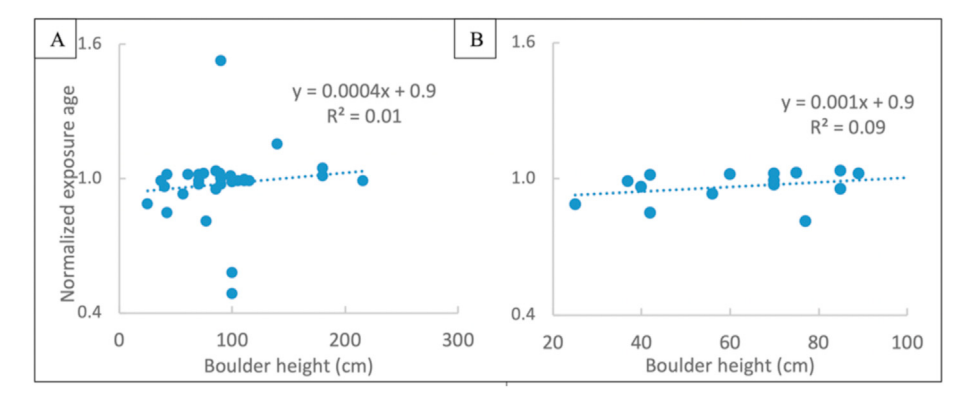


Fig. 7. Boulder height and exposure age. A. Boulder heights (maximum height, measured from the ground to where sample was taken from) and exposure age normalized to the moraine mean age, including outliers; B. Boulder height and exposure age for boulders under 90 cm high.

denudation (listed in order of the sample pairs shown in Fig. 4), which translates to moraine denudation rates of 8.0, 7.0, 10, 24, 40 mm per thousand years, if constant over the exposure histories.

Because of the wide range in these rates and the assumptions necessary for their calculation, we do not apply a denudation rate to our ages, but their discussion nonetheless provides relevant information for future sampling strategies. The wide range in denudation rates likely implies that exhumation, similar to erosion (see methods section), is probably not constant across boulders, and applying one rate to all of the boulders is inappropriate. While denudation likely affected our shorter boulders, the age difference between the shorter and taller boulders on the same landform in itself means that if denudation did impact the ages from the taller boulders, it is to a lesser degree. We do not have evidence for erosion or denudation affecting our tall boulders, and the young ages, which were likely affected by geomorphic processes, were removed from the means. The remaining ages from the MIS 4 moraines are internally or stratigraphically consistent as discussed above, leading us to infer that they were probably not impacted in a major way by geomorphic processes, which are likely to have a heterogeneous impact on the boulder surfaces.

6. Discussion

6.1. MIS 4 and 3 at Estrecho de Magallanes

Our results indicate that the Magallanes lobe reached its maximum extent of the last glacial cycle during MIS 4. Furthermore, our mapping and stratigraphically supported distribution of ages suggest several moraine building events occurred during MIS 4 (Fig. 3). The ages range from 67.5 ± 2.1 ka (n=3) to 62.1 ± 2.0 ka (n=1), although individual periods cannot be statistically distinguished from one another with existing data at 2σ . Although there are young outliers, which are likely the result of boulder-specific denudation or erosion (Fig. 4), the internal consistency of the dataset overall indicates the moraines formed during MIS 4, regardless of the uncertainties (Table 2).

The Magallanes lobe may have expanded at least towards the end of MIS 3 (Fig. 8). The 27.4 ± 0.8 ka moraine is much wider and taller than the rest of our MIS 2 moraines. This could indicate that

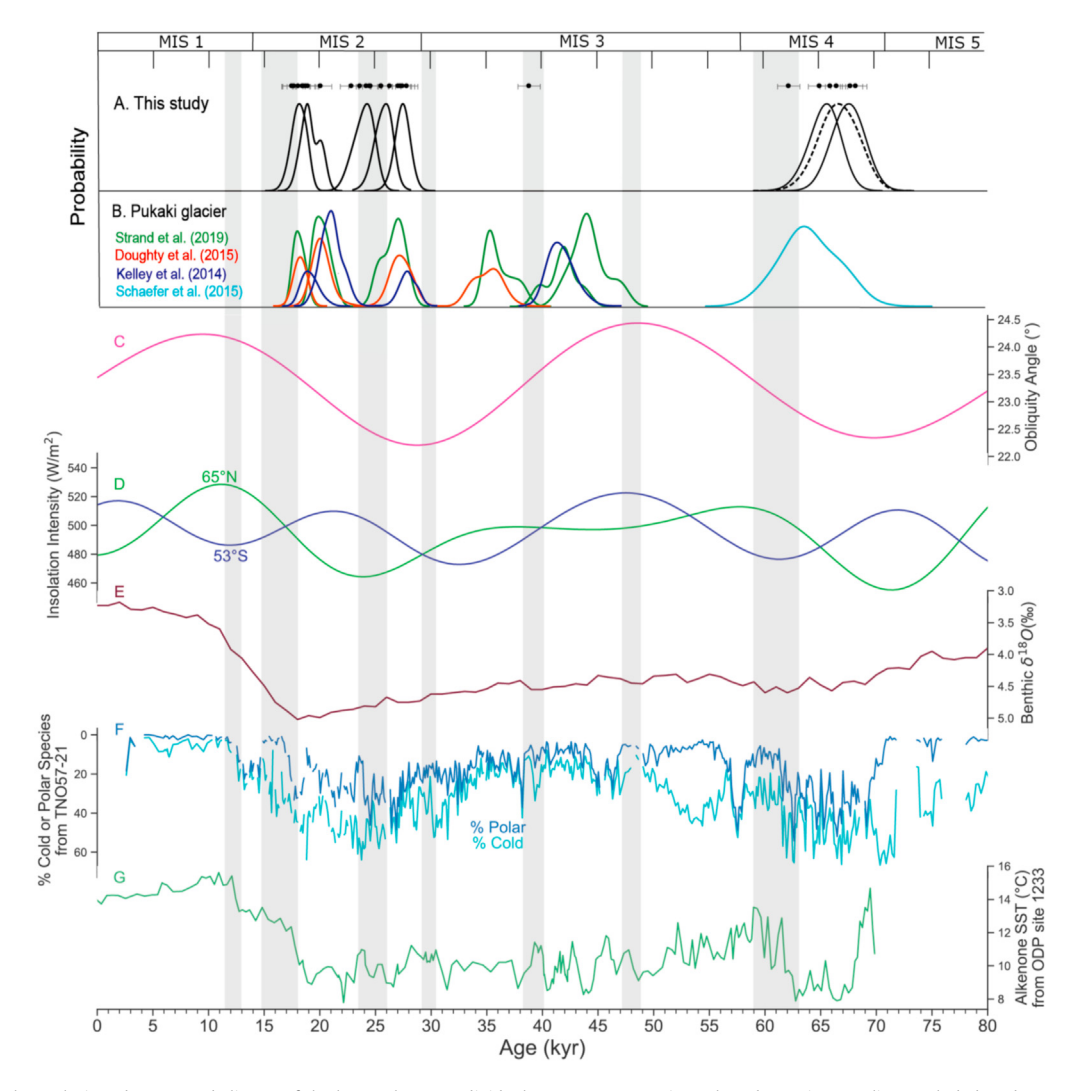


Fig. 8. Southern Hemisphere glacier advances and climate of the last 80 kyr. A. Individual ages $\pm 1\sigma$ uncertainty plotted as points, outliers excluded, and summed normal kernel density estimates of moraine ages. Dashed summed normal kernel density estimates shows all MIS 4 ages as one distribution (Fig. 7, 66.7 \pm 2.4 kyr. n = 5, 4 excluded), B. Summed normal kernel density estimates from the Pukaki glacier in New Zealand, C. Obliquity angle from Laskar et al. (2004), D. December 21st insolation at 53°S and June 21st insolation at 65°N (Laskar et al., 2004), E. The LR04 benthic δ180 stack from Lisiecki and Raymo (2005), F. Cold and polar planktonic foraminiferal species from the SE Atlantic core TN057-21 at 41°S, 8°E (Barker and Diz, 2014), G. Alkenone sea surface temperature from offshore Chile at ODP Site 1233 at 41°S, 74°E (Kaiser and Lamy, 2010). Vertical gray bars show the timing of Heinrich stadials based on speleothem records from China following Strand et al. (2019).

this moraine is a palimpsest landform that formed over multiple glacial stabilizations, or that the glacier sat at the 27.4 ± 0.8 ka margin over a long period. In addition, we infer the moraine boulders we sampled, which sit on the moraine surface, represent the final stages of moraine formation; hence the ice sheet lobe grew and advanced prior to 27.4 ± 0.8 ka. It is also possible that a MIS 3 advance reached the MIS 4 moraine; on the innermost edge of the mapped MIS 4 moraine, we have one age of 38.8 ± 0.7 ka (Fig. 3), which falls within MIS 3 and is coincident with nearby findings in southern Patagonia found by García et al. (2018) and ages reported by Sagredo et al. (2011). This inference is also supported by findings in northern Patagonia (Denton et al., 1999; Moreno et al., 2015) as well as at similar latitudes in New Zealand (e.g., Kelley et al., 2014; Doughty et al., 2015; Strand et al., 2019).

6.2. MIS 2 at Estrecho de Magallanes

We precisely dated 5 moraines within MIS 2, with multi-century precision, capturing the structure of the local LGM more finely than prior studies. 77% of the 34 ages in this study have analytical errors below 3%, which allows us to reconstruct the detailed internal structure of the MIS 2 glaciation in southern South America.

We find that the marginal deposits that appear to correspond to those that wrap around Primera Angostura date to MIS 2. This finding contrasts with earlier work that considered the moraines around Primera Angostura to be pre-LGM in age based on weathering characteristics and comparison with dated units elsewhere in Patagonia (e.g., Meglioli, 1992; Clapperton et al., 1995; Rabassa et al., 2000; McCulloch et al., 2005b). We suggest that Primera Angostura deposits show a higher degree of weathering due to proximity to the glacier margin for the following ~8 kyr as the lobe sat at its inboard positions. Recent mapping by Soteres et al. (2020) also concluded that the lobe reached Primera Angostura during MIS 2 (Fig. 2A). This is also supported by the reanalysis of four ¹⁰Be ages from around Primera Angostura from Kaplan et al. (2007) (Fig. 2A).

We find that the landforms just outboard of the moraines that terminate on Península Juan Mazía (what Clapperton et al. (1995) termed advance A and considered to be pre-LGM in age) do indeed capture multiple events (MIS 2 and MIS 4), a conclusion they draw based on relative weathering of the moraines (Clapperton et al., 1995; McCulloch et al., 2005b). This is particularly evident for the moraines on the north side of Segunda Angostura (Fig. 2A) which were previously mapped as part of advance A, but are inboard of what we now understand to be MIS 2 moraines based on the mapping of Soteres et al. (2020) in conjunction with our ages.

On Península Juan Mazía, there are at least three MIS 2 moraines that bifurcate and coalesce, and our mapping and chronology suggest that these landforms are all part of the same general moraine system. Less clear is the area between the Juan Mazía moraines and the Bahía Gente Grande moraines, as meltwater channels altered the original geomorphology, blurring the exact stratigraphic relationships with the rest of the mapped right lateral system to the south (Fig. 2B). We could be capturing an inner moraine system with our 18.1 \pm 0.6 ka age and an outer moraine system dated to 19.1 \pm 0.7 ka; additional data are needed to assess this inference. Regardless, the 10 Be ages suggest that the glacier was stable and forming moraines up until 18.1 \pm 0.6 ka.

The innermost moraine crests, which we infer are recessional based on the geomorphic setting (see Section 5.1), provide a maximum age for the deglaciation at 18.0 ± 0.8 ka. It is unlikely that the glacier sat at this innermost moraine for an extended period, in light of the scale of these ridges and the nearly identical 18.1 ± 0.6 ka age of the adjacent outboard moraine. It is possible that there was a small proglacial lake focused in the center of the strait before

this time, but any widespread post-glacial ice-dammed lakes did not form until after 18.0 ± 0.8 ka.

6.3. Estrecho de Magallanes record in a regional and hemispheric

We present one of the first directly dated MIS 4 records, and one of the most precise directly-dated MIS 2 records in southern South America. The Estrecho de Magallanes record, taken together with prior work, suggests that southern South America, and not just the Magallanes lobe, experienced a full glacial state during MIS 4 comparable to that during MIS 2. ~250 km to the north of Estrecho de Magallanes, three widely spaced ¹⁰Be ages of ~70 to 60 ka were produced from three different respective sites around Puerto Natales. These ages were considered outliers when originally published (Sagredo et al., 2011; García et al., 2018), but now, based on the finding of a MIS 4 advance at Estrecho de Magallanes and in New Zealand, perhaps these ages reflect MIS 4 advances. Pollen records from the Chilean Lake District (~40°S), ~1200 km to the north of Estrecho de Magallanes, show that climate conditions may have been similar during MIS 2 and 4 (Heusser et al., 2000; Heusser and Heusser, 2006).

Offshore data similarly suggest that sea surface temperatures during MIS 4 were as extreme as during MIS 2. Pollen data from the Ocean Drilling Program Site 1234 (~36°S, ~65 km offshore Chile; Fig. 1B) imply full glacial levels are reached during MIS 4, similar to MIS 2 and 6 (Heusser et al., 2006). The alkenone-based SST reconstruction from Ocean Drilling Program Site 1233 shows a prominent and long-lasting temperature low during MIS 4 (Fig. 8G. 1B; Kaiser and Lamy, 2010). A sediment core from the SE Atlantic Ocean (41°S, 8°E; Fig. 1A) shows abrupt cooling at the onset of MIS 4, similar in magnitude and rate to that of MIS 2 (Fig. 8F) (Barker and Diz, 2014). Interestingly, while South America is thought to be the dominant dust source to Antarctica (e.g., Grousset et al., 1992; Basile et al., 1997), including the Magallanes area specifically (Sugden et al., 2009), while there are peaks in Antarctic dust records during MIS 4, they are less extreme than during MIS 2. Because eustatic sea level was lower during MIS 2 than during MIS 4 (Siddall et al., 2003), one possible explanation is that more of the adjacent continental shelf was exposed during MIS 2, which was occupied by outwash plains, providing a source area of dust to Antarctica (e.g., Sugden et al., 2009).

Various proxies imply that MIS 4 climate was less extreme compared to MIS 2 (see section 3.2). Meanwhile, evidence that glaciers were more extensive during MIS 4 than MIS 2 is appearing from disparate locations. New Zealand's Pukaki dated moraine sequence shows indistinguishable timing to the Magallanes lobe during MIS 4 when ice was similarly larger than MIS 2. ¹⁰Be dating of the Pukaki glacier moraines reported by Schaefer et al. (2015) affords a mean age of 64.1 \pm 1.6 ka (n = 36, 3 outliers excluded) which overlaps with the Estrecho de Magallanes MIS 4 moraines at one standard deviation (Fig. 8B). Moreover, this finding is not limited to the Southern Hemisphere; in the Revelation Mountains in Alaska, Tulenko et al. (2018) found that glaciers were largest at 59.7 ± 3.6 ka (n = 9). Although additional records are needed to determine the global fingerprint of a MIS 4 glaciation more extensive than MIS 2, our results demonstrate that a broad sector of the southern mid-latitudes, ~8000 km apart between 44°S and 53°S (Fig. 1A), feature statistically identical 10Be ages for their MIS 4 glaciations.

Darvill et al. (2015) dated advances just south of Estrecho de Magallanes, in the adjacent Bahía Inútil-San Sebastián area, to 45.6 +139.9/-14.3 ka (Cullen profile) and 30.1 +45.6/-23.1 ka (Filaret profile), and they inferred these represented MIS 3 advances. Now that we know the Magallanes lobe has a major MIS 4

moraine preserved, it is possible that the Cullen and Filaret profile ages reflect an advance of the Bahía Inútil lobe during MIS 4, as the ages overlap within uncertainty. Alternatively, one or both profiles could indeed be MIS 3 in age as proposed by Darvill et al. (2015), especially given the occurrence of major MIS 3 advances in other Southern Hemisphere sites. Sagredo et al. (2011) reported two ages between ~40 and 35 ka from the Última Esperanza lobe 200 km to the north. García et al. (2018) subsequently dated moraines more comprehensively in the same area and at Torres del Paine to $47.8 \pm 1.5 \text{ ka}$ (n = 10), $38.9 \pm 1.4 \text{ ka}$ (n = 11), $33.8 \pm 1.1 \text{ ka}$ (n = 16), (we report median ages for this dataset following García et al., but otherwise we present these moraine ages according to our systematics as defined above), finding that the lobes were twice as extensive at 47.8 ± 2.3 ka than during the global LGM. In addition, a MIS 3 advance possibly occurred in the Estrecho de Magallanes area (section 6.1). Major MIS 3 advances have been identified in New Zealand starting around ~42 ka (Fig. 8B; e.g., Kelley et al., 2014; Doughty et al., 2015; Strand et al., 2019).

The Estrecho de Magallanes MIS 2 sequence is consistent with previously published glacier expansions from elsewhere in Patagonia (cf. Davies et al., 2020), although the uncertainties of ¹⁰Be ages in prior studies prevent robust one-to-one correlations between moraine building events. For example, Lago Buenos Aires (46.5°S) experienced culminations at 25.9 \pm 0.9, 25.8 \pm 1.2, 20.9 ± 1.2 , 19.6 ± 0.7 , and 18.3 ± 0.7 ka (Kaplan et al., 2004; Douglass et al., 2006). At the Lago Pueyrredón valley at 47.5°S, moraines are dated to 28.0 ± 1.0 , 24.6 ± 0.8 , and 20.8 ± 0.9 ka (Hein et al., 2010). Their oldest MIS 2 moraine is broadly consistent with that in the Estrecho de Magallanes record within uncertainty. Both Lago Buenos Aires and Pueyrredón valleys contain dated ~21 ka moraines but this advance is not observed in the study area, although we note that much of the Península Juan Mazía moraine landscape remains undated (Fig. 2). At all three sites the MIS 2 moraines cluster into two groups, one between ~28 and 24 ka and another between ~21 and 18 ka.

6.4. Climatic implications

During Heinrich stadials (episodes of extreme cold conditions in the North Atlantic) as the Atlantic Meridional Overturning Circulation slowed, the Intertropical Convergence Zone shifted south, as did the Subtropical Front and associated Southern Hemisphere Westerlies (Anderson et al., 2009; Denton et al., 2010; Barker and Diz, 2014). This likely brought more northern, warm climates to Cordillera Darwin leading to glacier retreat from the dated moraine limits (Figs. 2, 4 and 8). The end of the Magallanes MIS 4 maximum closely preceded Heinrich stadial 6 (Fig. 8), similar to the Pukaki glacier in New Zealand (Schaefer et al., 2015). The Estrecho de Magallanes study area has large scale geomorphic breaks between the MIS 4 and ~27.4 ka moraines, the ~27.4 and ~25.7 ka moraines, the ~23.9 and ~18.1 ka moraines, and after the ~18.1 ka moraine, indicating there was likely major glacier retreat during these four intervals. Heinrich stadials 1, 2, and 6 occur at the times where we find three out of four of these dated geomorphic breaks (Fig. 8). The Lago Buenos Aires record (Kaplan et al., 2004; Douglass et al., 2006) similarly shows clustering of moraines before Heinrich stadials 1 and 2. Recent work in New Zealand finds that the Pukaki glacier culminated between Heinrich stadials during MIS 2 and 3 (Fig. 8B; Strand et al., 2019).

Regarding the last termination, our record shows that the Magallanes lobe was stable until ~18.1 \pm 0.6 ka, and retreating at 18.0 \pm 0.8 ka, just before or ~ coeval with the start of the deglacial rise in CO₂ (Monnin et al., 2001; Marchitto et al., 2007; Marcott et al., 2014). Basal radiocarbon ages from bog cores in Seno Almirantazgo reported by Hall et al. (2013) imply that the Bahía

Inútil lobe (which shares an accumulation zone with the Magallanes lobe) retreated more than 150 km, all the way into Cordillera Darwin, by 16.8 ± 0.35 cal ka BP. This abrupt collapse of the ice sheet over Cordillera Darwin was in phase with Heinrich stadial 1, potentially reflecting a southward shift of the climate fronts over this area during the Northern Hemisphere Heinrich stadial 1 cooling (Hall et al., 2013). An offshore record from ODP Site 1233 at 41° S (Fig. 8F; Kaiser and Lamy, 2010), and the abrupt expansion of rainforest trees in continental sites at the same latitude (Moreno et al., 2015, 2018b; Moreno, 2020), are in agreement, and document rising sea surface and atmospheric temperatures during Heinrich stadial 1.

Researchers have hypothesized that the oceanic polar front and middle latitude westerly circulation shifted equatorward during the LGM (e.g., Heusser et al., 1996; Moreno et al., 1999; Lamy et al., 2004; Kohfeld et al., 2013), which could have exposed southern Patagonia to more polar-like climate conditions. An initial set of glaciological simulations using the University of Maine Ice Sheet Model (UMISM) suggests that ice could have expanded to dated moraines with mean annual temperature reductions of 4.5 °C for late MIS 2, 5.5 °C for early MIS 2, and at least 6 °C for MIS 4, if precipitation was reduced ~25% relative to present (see Supplementary Material for further discussion).

The Magallanes lobe stabilized in an expanded state at least 5 times during MIS 2, throughout half a cycle of insolation intensity, and the entire moraine sequence was deposited during rising and peaking local summer insolation intensity (Fig. 8D). The inconsistencies between the moraine chronology and mid-high latitude insolation intensity in either hemisphere leads us to cast doubt on the notion that summer insolation intensity (or a parameter intimately tied with it) played a major role in controlling glacier behavior in Estrecho de Magallanes. A similar finding was outlined by Doughty et al. (2015) for the Pukaki glacier in New Zealand, also in the middle latitudes of the Southern Hemisphere. On the other hand, we point out that the last two obliquity minima are centered at ~70 ka and 29 ka, around or just before our oldest MIS 4 and MIS 2 moraine ages (~2 and ~1 ka before, respectively; Fig. 8C). We propose that when obliquity is low, the subtropical and subantarctic fronts shift north, exposing the southern mid-latitudes to colder temperatures and allowing for the formation of extensive moraines during MIS 4, as well as early in MIS 2. Low obliquity, however, cannot explain the major MIS 3 advances of the Torres del Paine and Última Esperanza lobes (García et al., 2018), possibly of the Bahía Inútil-San Sebastián lobe (Darvill et al., 2015), and in New Zealand (Kelley et al., 2014; Doughty et al., 2015; Strand et al., 2019).

7. Conclusions

We report the first direct dating of a glaciation during MIS 4 in southern South America. We find that the Magallanes lobe was largest during the last glacial cycle at 67.5 ± 2.1 ka (n=3), meaning southern South America experienced a full glacial configuration during MIS 4, >40 kyr before Termination 1, similar to New Zealand's Southern Alps (Schaefer et al., 2015). The MIS 4 glacial maximum contained multiple advances, likely until close to ~62 ka. This suggests that climate during MIS 4 was similar to that of MIS 2, and this is likely a hemispheric, possibly global climate phenomenon rather than a small-scale local event unique to either New Zealand or Patagonia. In addition, South Atlantic and nearby South Pacific records indicate a MIS 4 of similar severity to MIS 2. Thus, mechanisms invoked to explain this event need to encompass at least all of the southern mid-latitudes and cannot be related only to local climate in one sector of the hemisphere.

Our results demonstrate that ridge-top erratics can reliably reflect moraine formation ages beyond MIS 2 in southern

Patagonia. Furthermore, we find that in dating older moraines, given a choice between sampling a short boulder (<~1 m) on the crest of a moraine or a tall boulder on the slope, the shorter boulder may be more likely to give a younger apparent age.

The results of this study support a long and punctuated local LGM, and improve our understanding of the MIS 2 glacier history of Patagonia. We find that the Magallanes lobe was in its full glacial configuration by ~27 ka and retreating at ~18 ka. Our new chronology allows us to see that during MIS 2 the Patagonian Ice Sheet at Estrecho de Magallanes expanded at least 5 times, throughout half a cycle of local insolation intensity. The entire moraine sequence was deposited during rising and peaking local summer insolation intensity. This implies that insolation intensity cannot explain all the variability in the fluctuation of the ice sheet. A similar result was documented in New Zealand (Kelley et al., 2014; Doughty et al., 2015) suggesting this is a hemisphere-wide phenomenon.

To explain the large MIS 4 and long MIS 2 found in southern Patagonia and elsewhere around the southern mid latitudes, we propose that on a hemispheric scale the polar frontal systems shifted equatorward during these intervals, exposing mid-latitude glaciers to persistent cold climates. The shift facilitated conditions that were ~5–6° colder, if precipitation was reduced slightly, relative to present, during MIS 2 and MIS 4 based on UMISM simulations. In addition, from a broad view, the last two glacial maxima at MIS 4 and 2 occurred soon after obliquity reached minima. On the other hand, during North Atlantic Heinrich stadials, the frontal systems in the Southern Hemisphere shifted poleward exposing Cordillera Darwin to more northerly-derived warm climates, which in two cases coincided with the end of glacial maxima.

CRediT authorship contribution statement

Carly Peltier: Conceptualization, Formal analysis, Investigation, Writing - original draft, Writing - review & editing. Michael R. Kaplan: Conceptualization, Formal analysis, Investigation, Writing - review & editing. Sean D. Birkel: Conceptualization, Formal analysis, Investigation, Writing - review & editing. Rodrigo L. Soteres: Investigation, Writing - review & editing. Esteban A. Sagredo: Investigation, Writing - review & editing. Juan Carlos Aravena: Investigation, Writing - review & editing. José Araos: Investigation. Patricio I. Moreno: Investigation, Writing - review & editing. Roseanne Schwartz: Methodology, Writing - review & editing. Joerg M. Schaefer: Conceptualization, Formal analysis, Investigation, Methodology, Writing - review & editing.

Declaration of competing interest

The authors declare that they have no known competing financial interests or personal relationships that could have appeared to influence the work reported in this paper.

Acknowledgments

The authors thank Alice Doughty for her thoughtful reading and valuable comments on the manuscript, Gonzalo Amigo, Paulina Ruiz Lobos, Inti González Ruiz, and Lucas Bianchi for their help in the field collecting samples, Jeremy Frisch and Jean Hanley for help processing samples, and Steve Barker for discussion. This is LDEO contribution #8486.

Funding

This work was supported by the National Science Foundation, NSF-BCS #1263474 (Kaplan, Schaefer) and #1263574 (Birkel) and

the LDEO and NASA GISS Climate Center. This work was also supported by funding from Fondecyt 1191435, DRI USA2013-0035, and the ANID Millennium Science Initiative/Millennium Nucleus Paleoclimate NCN17_079 (Moreno, Sagredo, Soteres). We also acknowledge the Fulbright Commission Visiting Scholar Grant (Kaplan), and Fulbright U.S. Student Grant (Peltier), and the National Ph.D. Fellowship grant CONICYT #21161417 (Soteres).

Appendix A. Supplementary data

Supplementary data to this article can be found online at https://doi.org/10.1016/j.quascirev.2021.106858.

References

- Anderson, R.F., Ali, S.B.T., Miller, L.I., Nielsen, S.H.H., Fleisher, M.Q., Anderson, B.E., Burckle, L.H., 2009. Wind-driven upwelling in the Southern Ocean and the deglacial rise in atmospheric CO2. Science 23, 1443e1448.
- Balco, G., Stone, J.O., Lifton, N.A., Dunai, T.J., 2008. A complete and easily accessible means of calculating surface exposure ages or erosion rates from 10Be and 26Al measurements. Quat. Geochronol. 3, 174–195.
- Barker, S., Diz, P., 2014. Timing of the descent into the last Ice Age determined by the bipolar seesaw. Paleoceanography 29 (6), 489–507.
- Basile, I., Grousset, F.E., Revel, M., Petit, J.R., Biscaye, P.E., Barkov, N.I., 1997. Patagonian origin of glacial dust deposited in East Antarctica (Vostok and Dome C) during glacial stages 2, 4 and 6. Earth Planet Sci. Lett. 146 (3–4), 573–589.
- Benn, D.I., Clapperton, C.M., 2000. Glacial sediment—landform associations and paleoclimate during the last glaciation, Estrecho de Magallanes, Chile. Quat. Res. 54 (1), 13–23.
- Bentley, M.J., Sugden, D.E., Hulton, N.R., McCulloch, R.D., 2005. The landforms and pattern of deglaciation in the Estrecho de Magallanes and Bahía Inútil, southernmost South America. Geogr. Ann. Phys. Geogr. 87 (2), 313–333.
- Broecker, W.S., 1978. The Cause of Glacial to Interglacial Climatic Change. inGautier, D., et al., Evolution of Planetary Atmospheres and Climatology of the Earth: Toulouse, France, Centre National d'Etudes Spatiales.
- Caldenius, C., 1932. Las glaciaciones cuaternarias en la Patagonia y Tierra del Fuego. Geogr. Ann. 14. 1–164.
- Caniupán, M., Lamy, F., Lange, C.B., Kaiser, J., Arz, H., Kilian, R., Baeza Urrea, O., Aracena, C., Hebbeln, D., Kissel, C., Laj, C., 2011. Millennial-scale sea surface temperature and Patagonian Ice Sheet changes off southernmost Chile (53 S) over the past~ 60 kyr. Paleoceanography 26 (3).
- Clapperton, C.M., Sugden, D.E., Kaufman, D.S., McCulloch, R.D., 1995. The last glaciation in central Magallanes Strait, southernmost Chile. Quat. Res. 44 (2), 133–148.
- Clark, P.U., Dyke, A.S., Shakun, J.D., Carlson, A.E., Clark, J., Wohlfarth, B., Mitrovica, J.X., Hostetler, S.W., McCabe, A.M., 2009. The last glacial maximum. Science 325 (5941), 710–714.
- CLIMAP Project Members, 1976. The Surface of the Ice-Age Earth. Science, pp. 1131–1137.
- CLIMAP Project, 1981. Seasonal Reconstructions of the Earth's Surface at the Last Glacial Maximum. Geological Society of America.
- Darvill, C.M., Stokes, C.R., Bentley, M.J., Lovell, H., 2014. A glacial geomorphological map of the southernmost ice lobes of Patagonia: the bahia inutil san sebastian, Magallanes, otway, skyring and rio gallegos lobes. J. Maps 10 (3), 500–520.
- Darvill, C.M., Bentley, M.J., Stokes, C.R., Hein, A.S., Rodés, Á., 2015. Extensive MIS 3 glaciation in southernmost Patagonia revealed by cosmogenic nuclide dating of outwash sediments. Earth Planet Sci. Lett. 429, 157–169.
- Davies J., B., Darvill M., C., Lovell, H., Bendle M., J., Dowdeswell A., J., Fabel, D., García, J.-L., Geiger, A., Glasser F., N., Gheorghiu M., D., Harrison, S., Hein S., A., Kaplan R., M., Martin R.V., J., Mendelova, M., Palmer, A., Pelto, M., Rodés, A., Sagredo A., E., Smedley K., R., Smellie L., J., Thorndycraft R., V., 2020. The evolution of the Patagonian Ice Sheet from 35 ka to the present day (PATICE). Earth-Science Reviews 204 j.earscirev.2020.103152.
- Denton, G.H., Heusser, C.J., Lowel, T.V., Moreno, P.I., Andersen, B.G., Heusser, L.E., Schlühter, C., Marchant, D.R., 1999. Interhemispheric linkage of paleoclimate during the last glaciation. Geogr. Ann. Phys. Geogr. 81 (2), 107–153.
- Denton, G.H., Anderson, R.F., Toggweiler, J.R., Edwards, R.L., Schaefer, J.M., Putnam, A.E., 2010. The last glacial termination. Science 328 (5986), 1652–1656.
- Doughty, A.M., Schaefer, J.M., Putnam, A.E., Denton, G.H., Kaplan, M.R., Barrell, D.J., Andersen, B.G., Kelley, S.E., Finkel, R.C., Schwartz, R., 2015. Mismatch of glacier extent and summer insolation in Southern Hemisphere mid-latitudes. Geology 43 (5), 407–410.
- Douglass, D.C., Singer, B.S., Ackert, M.R., Kaplan, M.R., Caffee, M.W., 2007. Constraining boulder erosion rates and ages of mid-Pleistocene morainesLago Buenos Aires, Argentina. GSA Abstracts and Programs Northeastern Section, 42nd Annual Meeting.
- Douglass, D.C., Singer, B.S., Kaplan, M.R., Mickelson, D.M., Caffee, M.W., 2006. Cosmogenic nuclide surface exposure dating of boulders on last-glacial and late-glacial moraines, Lago Buenos Aires, Argentina: interpretive strategies and paleoclimate implications. Quat. Geochronol. 1 (1), 43–58.

- Fastook, J.L., Mike, P., 1994. A finite-element model of Antarctica: sensitivity test for meteorological mass-balance relationship. J. Glaciol. 40 (134), 167–175.
- Fastook, J.L., Head, J.W., Marchant, D.R., Forget, F., 2008. Tropical mountain glaciers on Mars: altitude-dependence of ice accumulation, accumulation conditions, formation times, glacier dynamics, and implications for planetary spin-axis/ orbital history. Icarus 198 (2), 305–317.
- Fernández, R., Gulick, S., Rodrigo, C., Domack, E., Leventer, A., 2017. Seismic stratigraphy and glacial cycles in the inland passages of the Magallanes región of Chile, southernmost South America, Mar. Geol. 386, 19-31.
- García, J.L., Hein, A.S., Binnie, S.A., Gómez, G.A., González, M.A., Dunai, T.J., 2018. The MIS 3 maximum of the Torres del Paine and Última Esperanza ice lobes in Patagonia and the pacing of southern mountain glaciation. Quat. Sci. Rev. 185,
- Garreaud, R., Lopez, P., Minvielle, M., Rojas, M., 2013. Large-scale control on the Patagonian climate. J. Clim. 26 (1), 215–230.
- Gibbons, A.B., Megeath, I.D., Pierce, K.L., 1984. Probability of moraine survival in a succession of glacial advances. Geology 12 (6), 327-330.
- Grousset, F.E., Biscaye, P.E., Revel, M., Petit, J.R., Pye, K., Joussaume, S., Jouzel, J., 1992. Antarctic (Dome C) ice-core dust at 18 ky BP: isotopic constraints on origins. Earth Planet Sci. Lett. 111 (1), 175-182.
- Hall, B.L., Porter, C.T., Denton, G.H., Lowell, T.V., Bromley, G.R., 2013. Extensive recession of Cordillera Darwin glaciers in southernmost South America during Heinrich stadial 1. Quat. Sci. Rev. 62, 49-55.
- Hays, J.D., Imbrie, J., Shackleton, N.J., 1976. Variations in the Earth's orbit: pacemaker
- of the ice ages. Science 194 (4270), 1121–1132. Hein, A.S., Hulton, N.R., Dunai, T.J., Sugden, D.E., Kaplan, M.R., Xu, S., 2010. The chronology of the Last Glacial Maximum and deglacial events in central Argentine Patagonia. Quat. Sci. Rev. 29 (9-10), 1212-1227.
- Hervé, F., Fanning, C.M., Pankhurst, R.J., Mpodozis, C., Klepeis, K., Calderón, M., Thomson, S.N., 2010. Detrital zircon SHRIMP U-Pb age study of the Cordillera Darwin Metamorphic Complex of Tierra del Fuego: sedimentary sources and implications for the evolution of the Pacific margin of Gondwana. J. Geol. Soc. 167 (3), 555-568.
- Heusser, C.J., Lowell, T.V., Heusser, L.E., Hauser, A., Andersen, B.G., Denton, G.H., 1996. Full-glacial—late-glacial palaeoclimate of the Southern Andes: evidence from pollen, beetle and glacial records. J. Quat. Sci.: Publ. Quat. Res. Assoc. 11 (3), 173-184.
- Heusser, C.J., Lowell, T.V., Heusser, L.E., Moreira, A., Moreira, S., 2000. Pollen sequence from the Chilean Lake District during the llanquihue glaciation in marine oxygen isotope stages 4-2. J. Quat. Sci.: Publ. Quat. Res. Assoc. 15 (2), 115-125
- Heusser, C.J., Heusser, L.E., 2006. Submillennial palynology and palaeoecology of the last glaciation at Taiquemo (~ 50,000 cal yr, MIS 2-4) in southern Chile. Quat. Sci. Rev. 25 (5-6), 446-454.
- Heusser, L., Heusser, C., Mix, A., McManus, J., 2006. Chilean and Southeast Pacific paleoclimate variations during the last glacial cycle: directly correlated pollen and δ18O records from ODP Site 1234. Quat. Sci. Rev. 25 (23-24), 3404-3415.
- Hughes, P.D., Gibbard, P.L., Ehlers, J., 2013. Timing of glaciation during the last glacial cycle: evaluating the concept of a global 'Last Glacial Maximum'(LGM). Earth Sci. Rev. 125, 171-198.
- Jakobsson, M., Nilsson, J., Anderson, L., Backman, J., Björk, G., Cronin, T.M., Kirchner, N., Koshurnikov, A., Mayer, L., Noormets, R., O'Regan, M., 2016. Evidence for an ice shelf covering the central Arctic Ocean during the penultimate glaciation. Nat. Commun. 7, 10365.
- Jouzel, J., Barkov, N.I., Barnola, J.M., Bender, M., Chappellaz, J., Genthon, C., Kotlyakov, V.M., Lipenkov, V., Lorius, C.R.P.J., Petit, J.R., Raynaud, D., 1993. Extending the Vostok ice-core record of palaeoclimate to the penultimate glacial period. Nature 364 (6436), 407-412.
- Kaiser, J., Lamy, F., 2010. Links between Patagonian Ice Sheet fluctuations and Antarctic dust variability during the last glacial period (MIS 4-2). Quat. Sci. Rev. 29, 1464e1471.
- Kaplan, M.R., Ackert, R.P., Singer, B.S., Douglass, D.C., Kurz, M.D., 2004. Cosmogenic nuclide chronology of millennial-scale glacial advances during O-isotope stage 2 in Patagonia. GSA Bull. 116 (3-4), 308-321.
- Kaplan, M.R., Douglass, D.C., Singer, B.S., Ackert, R.P., Caffee, M.W., 2005. Cosmogenic nuclide chronology of pre-last glacial maximum moraines at Lago Buenos Aires, 46 S, Argentina. Quat. Res. 63 (3), 301–315.
- Kaplan, M.R., Coronato, A., Hulton, N.R.J., Rabassa, J.O., Kubik, P.W., Freeman, S.P.H.T., 2007. Cosmogenic nuclide measurements in southernmost South America and implications for landscape change. Geomorphology 87 (4), 284-301.
- Kaplan, M.R., Fogwill, C.J., Sugden, D.E., Hulton, N.R.J., Kubik, P.W., Freeman, S.P.H.T., 2008. Southern patagonian glacial chronology for the last glacial period and implications for southern ocean climate. Quat. Sci. Rev. 27 (3-4), 284-294.
- Kaplan, M.R., Strelin, J.A., Schaefer, J.M., Denton, G.H., Finkel, R.C., Schwartz, R., Putnam, A.E., Vandergoes, M.J., Goehring, B.M., Travis, S.G., 2011. In-situ cosmogenic 10Be production rate at Lago Argentino, Patagonia: implications for late-glacial climate chronology. Earth Planet Sci. Lett. 309, 21-32.
- Kelley, S.E., Kaplan, M.R., Schaefer, J.M., Andersen, B.G., Barrell, D.J.A., Putnam, A.E., Denton, G.H., Schwartz, R., Finkel, R.C., Doughty, A.M., 2014. High-precision 10Be chronology of moraines in the Southern Alps indicates synchronous cooling in Antarctica and New Zealand 42,000 years ago. Earth Planet Sci. Lett. 405, 194-206.
- Kohfeld, K.E., Graham, R.M., De Boer, A.M., Sime, L.C., Wolff, E.W., Le Quéré, C., Bopp, L., 2013. Southern Hemisphere westerly wind changes during the Last Glacial Maximum: paleo-data synthesis. Quat. Sci. Rev. 68, 76-95.

- Lal, D., 1991. Cosmic ray labeling of erosion surfaces: in situ nuclide production. Earth Planet Sci. Lett. 104, 424-439.
- Lamy, F., Kaiser, J., Ninnemann, U., Hebbeln, D., Arz, H.W., Stoner, J., 2004. Antarctic timing of surface water changes off Chile and Patagonian ice sheet response. Science 304 (5679), 1959-1962.
- Lambert, F., Bigler, M., Steffensen, J.P., Hutterli, M., Fischer, H., 2012. Centennial mineral dust variability in high-resolution ice core data from Dome C, Antarctica. Clim. Past 8 (2), 609.
- Laskar, I., Robutel, P., Joutel, F., Gastineau, M., Correia, A.C.M., Levrard, B., 2004. A long-term numerical solution for the insolation quantities of the Earth. Astron. Astrophys. 428, 261-285.
- Lifton, N., Sato, T., Dunai, T.J., 2014. Scaling in situ cosmogenic nuclide production rates using analytical approximations to atmospheric cosmic-ray fluxes. Earth Planet Sci. Lett. 386, 149-160.
- Lisiecki, L.E., Raymo, M.E., 2005. A Pliocene-Pleistocene stack of 57 globally distributed benthic delta O-18 records. Paleoceanography 20.
- Locarnini, R.A., Mishonov, A.V., Antonov, J.I., Boyer, T.P., Garcia, H.E., Baranova, O.K., Zweng, J.R., Johnson, 2010. In: Levitus, S. (Ed.), World Ocean Atlas 2009, Volume 1: Temperature, vol. 68. NOAA Atlas NESDIS, p. 184.
- Lovell, H., Stokes, C.R., Bentley, M.J., 2011. A glacial geomorphological map of the Seno Skyring-Seno Otway-Estrecho de Magallanes region, southernmost Patagonia. J. Maps 7 (1), 318-339.
- Marchitto, T.M., Lehman, S.J., Ortiz, J.D., Flückiger, J., van Geen, A., 2007. Marine radiocarbon evidence for the mechanism of deglacial atmospheric CO2 rise. Science 316 (5830), 1456-1459.
- Marcott, S.A., Bauska, T.K., Buizert, C., Steig, E.J., Rosen, J.L., Cuffey, K.M., Fudge, T.J., Severinghaus, J.P., Ahn, J., Kalk, M.L., McConnell, J.R., 2014. Centennial-scale changes in the global carbon cycle during the last deglaciation. Nature 514 (7524), 616-619.
- McCulloch, R.D., Bentley, M.J., 1998. Late glacial ice advances in the Estrecho de Magallanes, southern Chile. Quat. Sci. Rev. 17, 775-787.
- McCulloch, R.D., Bentley, M.J., Tipping, R.M., Clapperton, C.M., 2005a. Evidence for late-glacial ice dammed lakes in the central Estrecho de Magallanes and bahia inutil, southernmost South America. Geogr. Ann. Phys. Geogr. 87 (2), 335-362.
- McCulloch, R.D., Fogwill, C.J., Sugden, D.E., Bentley, M.J., Kubik, P.W., 2005b. Chronology of the last glaciation in central Estrecho de Magallanes and Bahía Inútil, southernmost South America. Geogr. Ann. Phys. Geogr. 87 (2), 289-312.
- Meglioli, A., 1992. Glacial geology of southernmost Patagonia, the Estrecho de Magallanes and northern Tierra del Fuego. Unpublished PhD Dissertation, Lehigh University, Bethlehem, PA, USA.
- Mercer, J.H., 1984. Simultaneous Climatic Change in Both Hemispheres and Similar Bipolar Interglacial Warming: Evidence and Implications. American Geophysical Union, pp. 307-313.
- Milankovitch, M.K., 1941. Kanon der Erdbestrahlung und seine Anwendung auf das Eiszeitenproblem. Royal Serbian Academy Special Publication, vol. 133. English, Translation published in 1969 by Israel Program for Scientific Translations, US Dept. Comm., pp. 1-633
- Mix, A.C., Bard, E., Schneider, R., 2001. Environmental processes of the ice age: land, oceans, glaciers (EPILOG). Quat. Sci. Rev. 20 (4), 627-657.
- Monnin, E., Indermühle, A., Dällenbach, A., Flückiger, J., Stauffer, B., Stocker, T.F., Raynaud, D., Barnola, J.M., 2001. Atmospheric CO2 concentrations over the last glacial termination. Science 291 (5501), 112-114.
- Moreno, P.I., Lowell, T.V., Jacobson Jr., G.L., Denton, G.H., 1999. Abrupt vegetation and climate changes during the last glacial maximum and last termination in the Chilean lake district: a case study from canal de la puntilla (41 s). Geogr. Ann. Phys. Geogr. 81 (2), 285-311.
- Moreno, P.I., Denton, G.H., Moreno, H., Lowell, T.V., Putnam, A.E., Kaplan, M.R., 2015. Radiocarbon chronology of the last glacial maximum and its termination in northwestern Patagonia. Quat. Sci. Rev. 122, 233-249.
- Moreno, P.I., Vilanova, I., Villa-Martínez, R., Dunbar, R.B., Mucciarone, D.A., Kaplan, M.R., Garreaud, R.D., Rojas, M., Moy, C.M., De Pol-Holz, R., Lambert, F., 2018a. Onset and evolution of southern annular mode-like changes at centennial timescale. Sci. Rep. 8 (1), 1-9.
- Moreno, P.I., Videla, J., Valero-Garcés, B., Alloway, B.V., Heusser, L.E., 2018b. A continuous record of vegetation, fire-regime and climatic changes in northwestern Patagonia spanning the last 25,000 years. Quat. Sci. Rev. 198, 15-36.
- Moreno, P.I., 2020. Timing and structure of vegetation, fire, and climate changes on the Pacific slope of northwestern Patagonia since the last glacial termination. Quat. Sci. Rev. 238, 106328.
- Nishiizumi, K., Imamura, M., Caffee, M.W., Southon, J.R., Finkel, R.C., McAninch, J., 2007. Absolute calibration of 10Be AMS standards. Nucl. Instrum. Methods Phys. Res. B 258, 403-413.
- Porter, S.C., 1990. Character and ages of Pleistocene drifts in a transect across the Estrecho de Magallanes. Quat. S. Am. Antarct. Peninsula 7, 35-50.
- Porter, S.C., Clapperton, C.M., Sugden, D.E., 1992. Chronology and dynamics of deglaciation along and near the Estrecho de Magallanes, southernmost South America. SGU series Ca. Res. Pap. 81, 233–239. Putnam, A.E., Schaefer, J.M., Barrell, D.J.A., Vandergoes, M., Denton, G.H.,
- Kaplan, M.R., Finkel, R.C., Schwartz, R., Goehring, B.M., Kelley, S.E., 2010. In situ cosmogenic 10Be production-rate calibration from the Southern Alps, New Zealand. Quat. Geochronol. 5 (4), 392-409.
- Rabassa, J., Coronato, A., Bujalesky, G., Salemme, M., Roig, C., Meglioli, A., Heusser, C., Gordillo, S., Roig, F., Borromei, A., Quattrocchio, M., 2000. Quaternary of Tierra del Fuego, southernmost South America: an updated review. Quat. Int. 68, 217-240.

- Roe, G., 2006. In defense of Milankovitch. Geophys. Res. Lett. 33 (24).
- Sagredo, E.A., Moreno, P.I., Villa-Martínez, R., Kaplan, M.R., Kubik, P.W., Stern, C.R., 2011. Fluctuations of the Última Esperanza ice lobe (52°S), Chilean Patagonia, during the last glacial maximum and termination. Geomorphology 125, 92–108
- Schaefer, J.M., Denton, G.H., Kaplan, M., Putnam, A., Finkel, R.C., Barrell, D.J., Andersen, B.G., Schwartz, R., Mackintosh, A., Chinn, T., Schlüchter, C., 2009. High-frequency Holocene glacier fluctuations in New Zealand differ from the northern signature. Science 324 (5927), 622–625.
- Schaefer, J.M., Putnam, A.E., Denton, G.H., Kaplan, M.R., Birkel, S., Doughty, A.M., Kelley, S., Barrell, D.J., Finkel, R.C., Winckler, G., Anderson, R.F., 2015. The southern glacial maximum 65,000 years ago and its unfinished termination. Quat. Sci. Rev. 114, 52–60.
- Schneider, C., Glaser, M., Kilian, R., Santana, A., Butorovic, N., Casassa, G., 2003. Weather observations across the southern Andes at 53 S. Phys. Geogr. 24 (2), 97–119
- Siddall, M., Rohling, E.J., Almogi-Labin, A., Hemleben, C., Meischner, D., Schmelzer, I., Smeed, D.A., 2003. Sea-level fluctuations during the last glacial cycle. Nature 423 (6942), 853–858.

- Soteres, R.L., Peltier, C., Kaplan, M.R., Sagredo, E.A., 2020. Glacial geomorphology of the Estrecho de Magallanes ice lobe, southernmost Patagonia, South America. J. Maps 16 (2), 299–312.
- Stone, J.O., 2000. Air pressure and cosmogenic isotope production. J. Geophys. Res.: Solid Earth 105 (B10), 23753–23759.
- Strand, P.D., Schaefer, J.M., Putnam, A.E., Denton, G.H., Barrell, D.J., Koffman, T.N., Schwartz, R., 2019. Millennial-scale pulsebeat of glaciation in the southern Alps of New Zealand. Quat. Sci. Rev. 220, 165–177.
- Sugden, D.E., McCulloch, R.D., Bory, A.J.M., Hein, A.S., 2009. Influence of Patagonian glaciers on Antarctic dust deposition during the last glacial period. Nat. Geosci. 2 (4), 281–285.
- Tulenko, J.P., Briner, J.P., Young, N.E., Schaefer, J.M., 2018. Beryllium-10 chronology of early and late wisconsinan moraines in the revelation Mountains, Alaska: insights into the forcing of wisconsinan glaciation in beringia. Quat. Sci. Rev. 197, 129—141.
- Zamora, E., Santana, A., 1979. Características climáticas de la costa Occidental de la Patagonia entre las latitudes 46° 40'y 56° 30'S. Anales del Instituto de la Patagonia.

Supplementary Material

2

3

4

5

6

7

8

9

10

11

12

13

14

15

16

17

18

19

20

21

22

23

1

SM 1.1 Glaciological Modeling

We reconstructed the Estrecho de Magallanes ice lobe using the University of Maine Ice Sheet Model (UMISM) (Fastook and Prentice, 1994; Fastook et al., 2008) and conducted sensitivity tests to examine possible MIS 2 and 4 climate regimes. UMISM is a 2D finite-element mass and momentum ice dynamics model that incorporates isostasy, thermodynamics, sliding, and a degree-day surface mass balance solver. The force balance in UMISM follows the shallow-ice approximation, whereby the driving stress is simplified to the product of the ice thickness and density, acceleration due to gravity, and ice surface slope (see SM 1.2 for general equations). A range of past climates is estimated by applying different combinations of sustained temperature and precipitation anomalies to the degree-day surface mass balance solver such that simulated ice can grow to within mapped moraines. Temperature and precipitation changes, ΔT (°C) and ΔP (%) relative to modern climate, are applied equally across the model domain. UMISM simulations begin with modern topographic boundary conditions from which glaciers form and expand depending on the supplied climatology. The base inputs to UMISM are a bed topography/bathymetry defining the simulation domain, and monthly mean temperature and precipitation fields for the degree-day surface mass balance solver (Fig. SM1). For bed topography we use 30 arcsecond GLOBE data (GLOBE, 1999) resampled to 1.2 km using bilinear interpolation. To account for bathymetry, which is not included in GLOBE, we overlaid resampled 1

arc-minute ETOPO1 data (NOAA, 2009) for all areas below present mean sea level. The

input temperature and precipitation fields for the surface mass-balance solver are defined by mean monthly 1981-2010 climatologies produced by averaging reanalysis outputs from NCEP CFSR (Saha et al., 2010) and ECMWF ERA5 (Dee et al., 2011). These reanalysis models were selected for the comparatively high resolution (~50 km), affording orographic precipitation rates across the Southern Andes in good accord with recent studies (Lenaerts et al., 2014; Krogh et al., 2015). The monthly temperature and precipitation grids are resampled to the 1.2 km resolution simulation domain using bilinear interpolation. Temperature is adjusted from the reanalysis resolution to the 1.2 km domain topography and simulated ice surfaces using a -5 °C/km atmospheric lapse rate at each model time integration.

Surface mass balance in UMISM is calculated using a degree-day method described in Putnam et al. (2013). Annual snow accumulation is calculated by summing precipitation amounts for all months where temperature is below freezing. Ablation totals are calculated by first summing melting degrees for all months where temperature is above freezing. Accumulated snow is then diminished at a prescribed snow melt rate, and any remaining melting degrees are then applied to melt ice at a prescribed ice melt rate. The snow and ice melt rates are 4.6 and 7.2 mm/degree day, respectively. These values are based on empirical determination for New Zealand (Anderson et al., 2006), and for simplicity we assume they may be applicable to southern South America.

The configuration and calibration of the glaciological model follows previous applications of UMISM to the Western U.S. and New Zealand Southern Alps (Birkel et al., 2012; Putnam et al., 2013; Schaefer et al., 2015). In particular, for simulations here we use a value of 0.03 for the sliding law constant, which from previous experimentation

affords a compromise between comparatively thin, fast-flowing and thick, slow-flowing ice. The Estrecho de Magallanes domain is complex and includes significant areas where paleo ice margins would have interfaced with ocean water, especially to the west of the mountain divide where ice likely expanded across the continental shelf. For simplicity, the sea level is fixed at 120 m below the modern datum to represent approximate MIS 2 conditions for the UMISM simulations. Moreover, to reduce the degrees of freedom in the simulation, a simple calving parameterization is used whereby mass flux is enhanced at the grounding-line where the water depth exceeds 500 m relative to MIS 2 sea level, ensuring that ice can expand only to the continental shelf edge. The paleo ice lobes that expanded over shallow basins east of the mountain divide in the Estrecho de Magallanes domain are unaffected by this calving parameterization, and therefore ice extent reflects the driving climatology and surface mass balance. We assume these model configurations are reasonable, given that the intent of the simulations are to test possible paleo climate regimes that could support expansive ice, rather than deglaciation scenarios in which calving would become an important factor as ice margins retreated into over-deepened lake basins.

63

64

65

66

67

68

47

48

49

50

51

52

53

54

55

56

57

58

59

60

61

62

SM 1.2 Overview of equations

A complete description of UMISM can be found in Fastook and Prentice (1994) and Fastook et al. (2008). Here we provide an overview of the general equations used for the model ice-flow solver. First, the core of UMISM is a differential equation for ice extent and thickness as a function of time derived from an integrated momentum

conservation equation based on the flow law of ice (Glen, 1955), coupled with a continuity equation for mass conservation:

72
$$\frac{\delta h}{\delta t} = MB - \nabla \cdot (UH), \quad (1)$$

where $\delta h/\delta t$ is the time-dependent ice-surface elevation, MB is the net-annual surface mass balance (accumulation minus ablation), U is the column-average ice velocity, and H is the ice thickness.

U in Equation 1 is obtained by expanding:

$$\dot{\mathcal{E}} = \left[\frac{\sigma}{A}\right]^n, \quad (2)$$

which is a tensor equation expressing strain rates, $\dot{\mathcal{E}}$, and stresses, σ , through a non-linear power law. In this equation, n is the empirical flow law constant [we use a value of 3 for temperate glaciers (Paterson, 1994)], and A is a temperature dependent function that represents ice hardness in an Arrhenius relationship:

$$A = EA_0 e^{-Q/RT}, \quad (3)$$

where A0 is a constant, Q is the activation energy for ice creep, R is the gas constant, T is the ice temperature, and E is a tuning (or flow enhancement) parameter meant to account for ice impurities.

By shallow-ice approximation, all stresses and strain rates are ignored in the force balance except basal drag. Thus, the stress in Equation 2 acting on the bed, or the "driving" stress, is expressed:

96
$$\sigma_{xz} = \rho g H \nabla h, \quad (4)$$

where σ_{xz} is a stress in the x-direction acting on a surface with normal in the z direction, ρ is density of ice, g is gravitational acceleration, H is ice thickness, and ∇h is ice-surface slope.

Finally, *U*, is calculated from the sum of velocity due to internal deformation, *UD*, and velocity due to basal sliding, *US*, as expressed:

104
$$U = U_D + U_S = \frac{2}{n+2} \left[\frac{\rho g \nabla h}{A} \right]^n H^{n+1} + \left[\frac{\rho g \nabla h}{B} \right]^m H^m, \quad (5)$$

where the last term follows a general sliding law relationship developed by Weertman (1964) for beds at the melting point, and modified to incorporate the effect of basal water (Johnson and Fastook, 2002). Here n is the empirical flow law constant in Equation 2, A is the ice hardness parameter described in Equation 3, B is the sliding law constant, and B is the sliding law exponent.

112

113

114

115

116

117

118

119

120

121

122

123

124

125

126

127

128

129

130

131

132

133

SM 1.3 Experiment Results

A series of UMISM experiments were conducted to examine the growth of the ice sheet complex across the Estrecho de Magallanes region under different temperature (ΔT) and precipitation (ΔP) climate regimes. The experiments begin with modern topographic boundary conditions and are run for 5,000 years for ice margins to attain approximate equilibrium with the imposed temperature and precipitation. For simplicity, here we focus on simulations for which $\Delta P = 25\%$ and where temperature is varied in increments of 0.5 °C. The results indicate that ice expanded to mapped moraines driven by $\Delta T = -4.5$ °C for late MIS 2, $\Delta T = -5.5$ °C for early MIS 2, and at least $\Delta T = -6$ °C for MIS 4 (**Fig.** SM 2). Our results for MIS 2 are consistent with observation-based estimates for temperature reduction in Patagonia of ~5 to 6 °C (Denton et al. 1999; Hulton et al., 2002). Our simulated estimates are essentially indistinguishable (-5.5 °C for early LGM) from the ΔT -6 °C found in an earlier modeling study by Hulton et al. (2002). We also highlight the fundamentally different nature of the simulations in Hulton et al. (2002) and their (earlier) modeled results for the Magallanes area. We note that a caveat to our results is the inability of UMISM, at least as configured, to channel the eastward expanding ice lobes into distinct basins as mapped for climates colder than present during the LGM. Instead, ice consistently overtops the low plateau between Estrecho de Magallanes and Inútil Bay for ΔT values cooler than -5

°C. This unrealistic outcome may stem from either limitations of the shallow ice

approximation in UMISM, or the need for a higher resolution domain. Further glaciological modeling could examine these points, as well as test other surface mass balance methods.

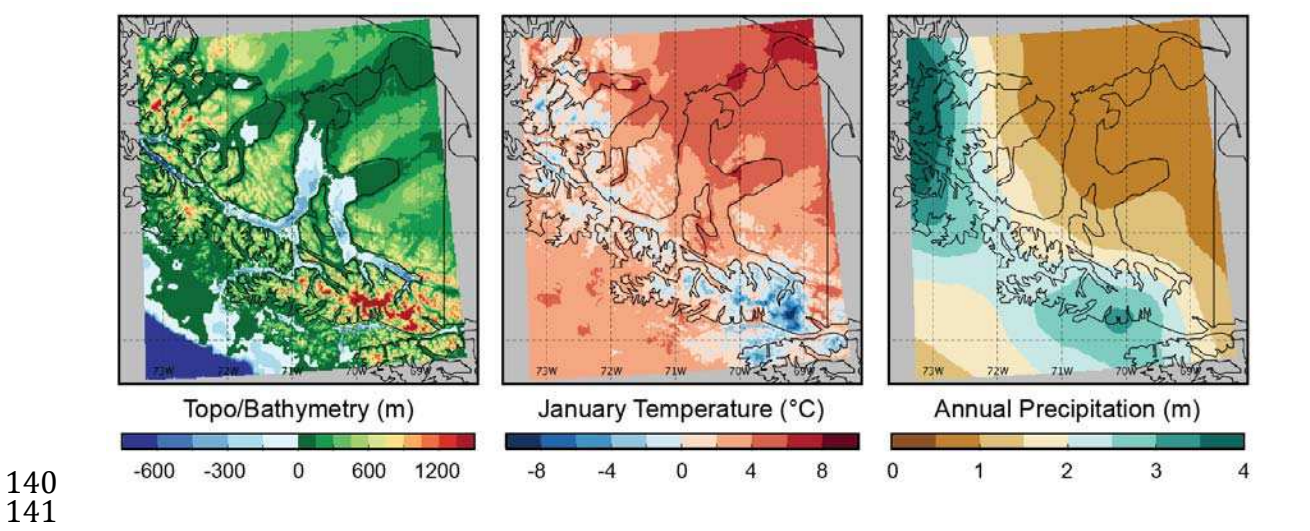


Figure SM1. Primary inputs to the glaciological model: a) topography and bathymetry, and mean monthly b) temperature (January shown) and c) precipitation (annual shown) climatology.

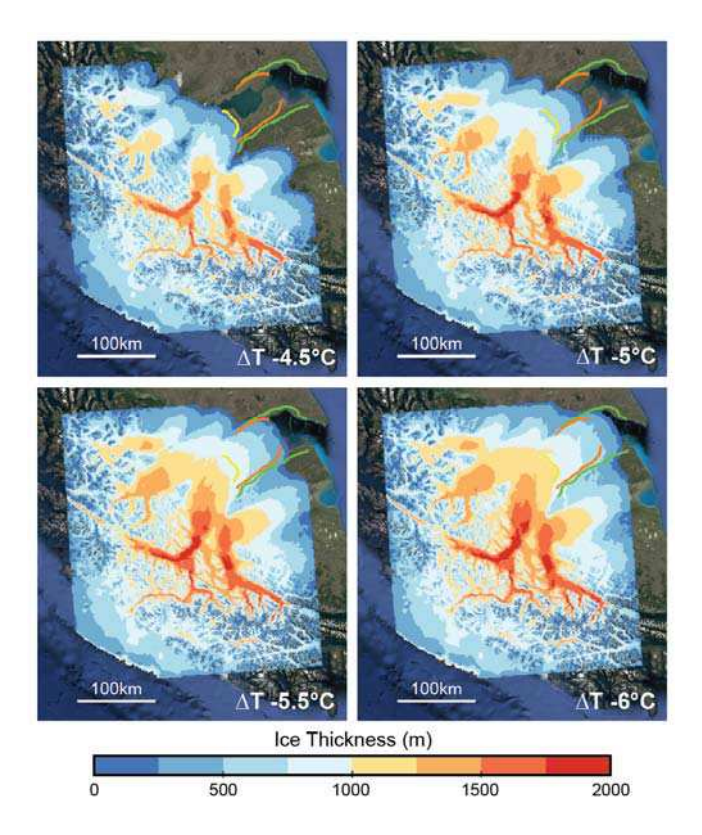


Figure SM2. UMISM ice thickness results for experiments where ΔT is varied from -4.5 °C to -6 °C in increments of 0.5 °C, and where precipitation is held fixed at 25% less than modern climatology. Each solution is taken at 5,000 model years and shows the ice in approximate equilibrium with the climate forcing. Target moraines mapped in this study are shown in yellow (late MIS 2), orange (early MIS 2), and green (MIS 4). The base map is from Google Earth.

References

Anderson, B., Lawson, W., Owens, I., Goodsell, B., 2006. Past and future mass balance of 'Ka Roimata o Hine Hukatere' Franz Josef Glacier, New Zealand. Journal of Glaciology 52 (179), 597-607.

Dee, D.P., Uppala, S.M., Simmons, A.J., Berrisford, P., Poli, P., Kobayashi, S., Andrae, U., Balmaseda, M.A., Balsamo, G., Bauer, D.P. and Bechtold, P., 2011. The ERA-Interim reanalysis: Configuration and performance of the data assimilation system. Quarterly Journal of the royal meteorological society, 137(656), pp.553-597.

Fastook, J.L. and Mike, P., 1994. A finite-element model of Antarctica: sensitivity test for meteorological mass-balance relationship. Journal of Glaciology, 40(134), pp.167-175.

Fastook, J.L., Head, J.W., Marchant, D.R. and Forget, F., 2008. Tropical mountain glaciers on Mars: Altitude-dependence of ice accumulation, accumulation conditions,

- formation times, glacier dynamics, and implications for planetary spin-axis/orbital
- 174 history. Icarus, 198(2), pp.305-317.

175

- 176 GLOBE Task Team and others (Hastings, David A., Paula K. Dunbar, Gerald M.
- 177 Elphingstone, Mark Bootz, Hiroshi Murakami, Hiroshi Maruyama, Hiroshi Masaharu,
- 178 Peter Holland, John Payne, Nevin A. Bryant, Thomas L. Logan, J.-P. Muller, Gunter
- 179 Schreier, and John S. MacDonald), eds., 1999. The Global Land One-kilometer Base
- 180 Elevation (GLOBE) Digital Elevation Model, Version 1.0. National Oceanic and
- 181 Atmospheric Administration, National Geophysical Data Center, 325 Broadway,
- Boulder, Colorado 80305-3328, U.S.A. Digital data base on the World Wide Web (URL:
- https://www.ngdc.noaa.gov/mgg/topo/globe.html) and CD-ROMs.

184

- 185 Krogh, S.A., Pomeroy, J.W., McPhee, J., 2015. Physically based mountain hydrological
- modeling using reanalysis data in Patagonia. Journal of Hydrometeorology 16, 172-193,
- 187 doi:10.1175/JHM-D-13-0178.1.

188

- Lenaerts, J.T.M. et al., 2014. Extreme precipitation and climate gradients in Patagonia
- revealed by high-resolution regional atmospheric climate modeling. Journal of Climate
- 191 27, 4607-4621, doi:10.1175/JCLI-D-13-00579.1.

192

- NOAA National Geophysical Data Center. 2009: ETOPO1 1 Arc-Minute Global Relief
- 194 Model. NOAA National Centers for Environmental Information.
- 195 doi:10.7289/V5C8276M.

196

200

- Saha, S., Moorthi, S., Pan, H.L., Wu, X., Wang, J., Nadiga, S., Tripp, P., Kistler, R.,
- Woollen, J., Behringer, D. and Liu, H., 2010. The NCEP climate forecast system
- reanalysis. Bulletin of the American Meteorological Society, 91(8), pp.1015-1058.